Quantitative Effects of Ion Pairing and Sterics on Chain Propagation Kinetics for 1-Hexene Polymerization Catalyzed by Mixed Cp′/ArO Complexes

Thomas A. Manz,[†] Shalini Sharma,[‡] Khamphee Phomphrai,[‡] Krista A. Novstrup,[†] Andrew E. Fenwick,[‡] Phillip E. Fanwick,[‡] Grigori A. Medvedev,[†] Mahdi M. Abu-Omar,[‡] W. Nicholas Delgass,[†] Kendall T. Thomson,[†] and James M. Caruthers*,[†]

School of Chemical Engineering and Department of Chemistry, Purdue University, West Lafayette, Indiana 47907

Received June 1, 2008

A series of single-site catalysts with mixed cyclopentadienyl/aryloxide ligation were synthesized and used to polymerize 1-hexene. The effects of solvent, metal, counterion, and ligand structure were investigated by experiments and by DFT calculations. A solvent with a high dielectric constant led not only to an increase in the chain propagation rate but also to a change in the reaction order. Catalyst reactivity was found to be controlled by the difficulty of ion pair separation and steric congestion at the metal center, which were quantified from DFT simulation by SCF ion pair separation energies and ligand cone angles. A Cp*Ti(OC_6H_4-2-Br)Me_2/B(C_6F_5)$_3$ catalyst exhibits unusually high reactivity, which was correlated to the formation of a partial bond between the aryloxide ortho substituent bromide and Ti upon ion pair separation. Natural bond orbital analysis was used to quantify the order of this opportunistic ligation for a series of catalysts. Kinetic analysis and a structure−activity correlation were applied to interpret the experimental results.

Introduction

Homogeneous single-site olefin polymerization catalysts are commercially important because the catalyst structure can be engineered to control the polymer molecular weight distribution and tacticity.[1,2] These complexes contain a transition metal bound to organic ligands and are often used to polymerize olefins in the condensed phase. Most commonly these complexes consist of a positively charged metal ion of group IV associated with a bulky and weakly coordinating counteranion.

It has been established that the nature of the counterion has a large effect on catalyst reactivity and stereoselectivity,[3−5] as reviewed by Chen and Marks[6] and Pedeutour et al.[7] Marks and co-workers have shown that the counterion needs to be weakly coordinating to achieve high catalyst activity.[3,6] In order for the monomer to reach the catalytic site, the counterion must be partially displaced; thus, a weakly bound counterion facilitates monomer coordination and insertion. Ziegler et al. and Fragala et al. have used computational chemistry to study the effects of solvent on ion pair formation and separation energies[8,9] as well as on reaction barriers for chain initiation and propagation.[10] The presence of solvent was found to dramatically lower the ion pair separation energies and overall chain propagation barriers. Since partial separation of the ion pair occurs in the transition states for chain propagation, the lower barriers to chain propagation in the presence of solvent were presumably due to lower ion pair separation energies.

A key question is how to quantitatively model structure−activity relationships in single-site olefin polymerization catalysis. While it is known that lower ion pair separation energies and higher solvent dielectric constants can enhance polymerization activity, only recently Manz et al. presented a quantitative model explaining how much the chain propagation rate constant increases for a given change in ligand structure.[11] An important question is whether the structure−activity correlation of Manz et al. can be extended to include changes in metal, counterion, and solvent.

* To whom correspondence should be addressed. E-mail: caruther@ecn.purdue.edu.

[†] School of Chemical Engineering.

[‡] Department of Chemistry.

(1) (a) Alt, H. G.; Koppl, A. *Chem. Rev.* **2000**, *100*, 1205–1221. (b) Coates, G. W.; Hustad, P. D.; Reinartz, S. *Angew. Chem., Int. Ed.* **2002**, *41*, 2236–2257.

(2) *Chem. Rev.* **2000**, *100* (entire issue No. 4).

(3) Chen, M. C.; Roberts, J. A. S.; Marks, T. J. *J. Am. Chem. Soc.* **2004**, *126*, 4605–4625.

(4) (a) Wilson, P. A.; Hannant, M. H.; Wright, J. A.; Cannon, R. D.; Bochmann, M. *Macromol. Symp.* **2006**, *236*, 100–110. (b) Deck, P. A.; Beswick, C. L.; Marks, T. J. *J. Am. Chem. Soc.* **1998**, *120*, 12167–12167. (c) Luo, L.; Marks, T. J. *Top. Catal.* **1999**, *7*, 97–106.

(5) (a) Yang, X. M.; Stern, C. L.; Marks, T. J. *J. Am. Chem. Soc.* **1994**, *116*, 10015–10031. (b) Jia, L.; Yang, X. M.; Ishihara, A.; Marks, T. J. *Organometallics* **1995**, *14*, 3135–3137. (c) Chen, M. C.; Roberts, J. A. S.; Marks, T. J. *Organometallics* **2004**, *23*, 932–935. (d) Metz, M. V.; Schwartz, D. J.; Stern, C. L.; Marks, T. J.; Nickias, P. N. *Organometallics* **2002**, *21*, 4159–4168. (e) Metz, M. V.; Sun, Y. M.; Stern, C. L.; Marks, T. J. *Organometallics* **2002**, *21*, 3691–3702.

(6) Chen, E. Y. X.; Marks, T. J. *Chem. Rev.* **2000**, *100*, 1391–1434.

(7) Pedeutour, J. N.; Radhakrishnan, K.; Cramail, H.; Deffieux, A. *Macromol. Rapid Commun.* **2001**, *22*, 1095–1123.

(8) (a) Lanza, G.; Fragala, I. L.; Marks, T. J. *J. Am. Chem. Soc.* **1998**, *120*, 8257–8258. (b) Xu, Z. T.; Vanka, K.; Firman, T.; Michalak, A.; Zurek, E.; Zhu, C. B.; Ziegler, T. *Organometallics* **2002**, *21*, 2444–2453.

(9) (a) Chan, M. S. W.; Vanka, K.; Pye, C. C.; Ziegler, T. *Organometallics* **1999**, *18*, 4624–4636. (b) Lanza, G.; Fragala, I. L.; Marks, T. J. *J. Am. Chem. Soc.* **2000**, *122*, 12764–12777. (c) Vanka, K.; Chan, M. S. W.; Pye, C. C.; Ziegler, T. *Organometallics* **2000**, *19*, 1841–1849.

(10) (a) Lanza, G.; Fragala, I. L. *Top. Catal.* **1999**, *7*, 45–60. (b) Lanza, G.; Fragala, I. L.; Marks, T. J. *Organometallics* **2002**, *21*, 5594–5612. (c) Xu, Z. T.; Vanka, K.; Ziegler, T. *Organometallics* **2004**, *23*, 104–116.

(11) Manz, T. A.; Phomphrai, K.; Medvedev, G.; Krishnamurthy, B. B.; Sharma, S.; Haq, J.; Novstrup, K. A.; Thomson, K. T.; Delgass, W. N.; Caruthers, J. M.; Abu-Omar, M. M. *J. Am. Chem. Soc.* **2007**, *129*, 3776–3777.

(12) Macchioni, A. *Chem. Rev.* **2005**, *105*, 2039–2073.

10.1021/om8004993 CCC: $40.75
Publication on Web 10/08/2008

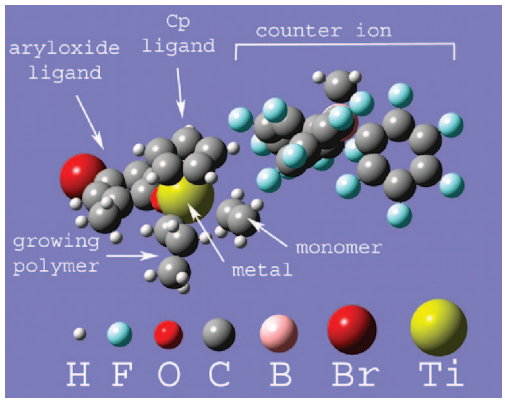

Figure 1. Example of a single-site olefin polymerization catalyst containing mixed cyclopentadienyl/aryloxide ligation: the front-side ethylene π-complex of $[CpTi(OC_6H_3\text{-}2,6\text{-}Me_2\text{-}4\text{-}Br)C_3H_7]^+[MeB(C_6F_5)_3]^-$.

Another important question is what roles different forms of the ion pair play in the polymerization kinetics. Macchioni reviewed ion pairing in transition-metal organometallic chemistry, including olefin polymerization.[12] Four types of transition-metal ion pairs were discussed: (a) an inner-sphere ion pair (ISIP) in which the counterion exists in the first coordination sphere of the metal, (b) an outer-sphere ion pair (OSIP) in which the counterion exists in the second coordination sphere of the metal, (c) a solvent-shared ion pair or solvated cation−anion pair (SCAP) in which a single solvent layer separates the cation from the counterion, and (d) a solvent-separated ion pair (SSIP) in which two or more solvent layers separate the cation from the counterion. All four of these ion pair types have been experimentally and computationally observed for some single-site olefin polymerization systems.[9,13−17] Which ion pair type is the most favored depends upon the catalyst structure, solvent, and other reaction conditions. In addition, aggregates consisting of four, eight, or more ions in a cluster are possible and have been experimentally observed at higher catalyst concentrations,[15,17] but some studies indicate that aggregates are not likely to form at the low catalyst concentrations typically employed in polymerization reactions.[17,18] Different forms of each of these ion pair types are also possible. For example, an OSIP may exist with or without agostic bonding between the growing polymer chain and metal center, and several papers have investigated the details of these agostic interactions.[15,19]

In order to address these two key questions, we now report experimental and DFT results for a series of Ti and Zr catalysts containing mixed cyclopentadienyl/aryloxide ligation. Dimethyl catalyst precursors were activated with $B(C_6F_5)_3$ or $Ph_3CB(C_6F_5)_4$. An example of a catalyst is shown in Figure 1, where the counterion is displaced from the metal center and turned sideways to allow room for the monomer to dock.

Ti/Zr mixed Cp′/ArO catalysts have been used to polymerize 1-hexene,[11,20−23] propylene,[16,21,24,25] ethylene,[16,21,24−28] and styrene,[22,24,29] and these catalysts are well suited for copolymerization involving ethylene/1-hexene,[21,28,30] ethylene/1-butene,[21,26] ethylene/styrene,[31] ethylene/cyclohexene,[32] and ethylene/norbornene.[33] Most of these studies focused on activation of the dichloride precursors by methylaluminoxane (MAO). Changes in the ligand structure were found to affect the polymerization rate, polymer molecular weight, and degree of comonomer incorporation. Nomura and co-workers, who have done extensive work on these catalyst systems and written a review of them,[34] have recently developed a method for tethering mixed Cp′/ArO catalysts and found that the tethered catalysts have catalytic properties similar to those of the untethered species.[35] Polymerization catalysts have also been synthesized with a bridge connecting the Cp′ and ArO ligands.[24,36] On the basis of this data, mixed Cp′/ArO ligated catalysts afford a number of advantages for detailed kinetic studies. First, they are active for the polymerization of 1-hexene, which allows the monomer to be added in the liquid phase close to ambient temperature and pressure. Second, the structure of the aryloxide ligand can be conveniently varied, owing to the availability of different phenols. Finally, changing the structure of the aryloxide ligand allows the electronic and steric properties of these catalysts to be systematically tuned.

There are five basic ways we will vary the ion pair behavior in the Ti/Zr mixed Cp′/ArO systems: (a) change the metal, (b) change the solvent, (c) change the ligands to alter steric and electronic properties, (d) change the activator/counterion, and

(13) Bochmann, M.; Cannon, R. D.; Song, F. *Kinet. Catal.* **2006**, *47*, 160–169.
(14) Eisch, J. J.; Pombrik, S. I.; Zheng, G. X. *Organometallics* **1993**, *12*, 3856–3863.
(15) Song, F. Q.; Lancaster, S. J.; Cannon, R. D.; Schormann, M.; Humphrey, S. M.; Zuccaccia, C.; Macchioni, A.; Bochmann, M. *Organometallics* **2005**, *24*, 1315–1328.
(16) Tremblay, T. L.; Ewart, S. W.; Sarsfield, M. J.; Baird, M. C. *Chem. Commun.* **1997**, 831–832.
(17) Zuccaccia, C.; Stahl, N. G.; Macchioni, A.; Chen, M. C.; Roberts, J. A.; Marks, T. J. *J. Am. Chem. Soc.* **2004**, *126*, 1448–1464.
(18) Stahl, N. G.; Zuccaccia, C.; Jensen, T. R.; Marks, T. J. *J. Am. Chem. Soc.* **2003**, *125*, 5256–5257.
(19) (a) Brookhart, M.; Green, M. L. H.; Parkin, G. *Proc. Natl. Acad. Sci. USA* **2007**, *104*, 6908–6914. (b) Nifant'ev, I. E.; Ustynyuk, L. Y.; Laikov, D. N. *Organometallics* **2001**, *20*, 5375–5393.
(20) (a) Nomura, K.; Fudo, A. *Inorg. Chim. Acta* **2003**, *345*, 37–43. (b) Nomura, K.; Fudo, A. *J. Mol. Catal. A: Chem.* **2004**, *209*, 9–17.
(21) Nomura, K.; Naga, N.; Miki, M.; Yanagi, K.; Imai, A. *Organometallics* **1998**, *17*, 2152–2154.
(22) Nomura, K.; Tanaka, A.; Katao, S. *J. Mol. Catal. A: Chem.* **2006**, *254*, 197–205.
(23) Phomphrai, K.; Fenwick, A. E.; Sharma, S.; Fanwick, P. E.; Caruthers, J. M.; Delgass, W. N.; Abu-Omar, M. M.; Rothwell, I. P. *Organometallics* **2006**, *25*, 214–220.
(24) Chen, Y. X.; Fu, P. F.; Stern, C. L.; Marks, T. J. *Organometallics* **1997**, *16*, 5958–5963.
(25) Ewart, S. W.; Sarsfield, M. J.; Jeremic, D.; Tremblay, T. L.; Williams, E. F.; Baird, M. C. *Organometallics* **1998**, *17*, 1502–1510.
(26) Nomura, K.; Naga, N.; Miki, M.; Yanagi, K. *Macromolecules* **1998**, *31*, 7588–7597.
(27) (a) Antinolo, A.; Carrillo-Hermosilla, F.; Corrochano, A.; Fernandez-Baeza, J.; Lara-Sanchez, A.; Ribeiro, M. R.; Lanfranchi, M.; Otero, A.; Pellinghelli, M. A.; Portela, M. F.; Santos, J. V. *Organometallics* **2000**, *19*, 2837–2843. (b) Zhang, Y. T.; Mu, Y.; Lu, C. S.; Li, G. H.; Xu, J. S.; Zhang, Y. R.; Zhu, D. S.; Feng, S. H. *Organometallics* **2004**, *23*, 540–546.
(28) (a) Rau, A.; Schmitz, S.; Luft, G. *J. Organomet. Chem.* **2000**, *608*, 71–75. (b) Zhang, Y. T.; Wang, J. H.; Mu, Y.; Shi, Z.; Lu, C. S.; Zhang, Y. R.; Qiao, L. J.; Feng, S. H. *Organometallics* **2003**, *22*, 3877–3883.
(29) (a) Byun, D. J.; Fudo, A.; Tanaka, A.; Fujiki, M.; Nomura, K. *Macromolecules* **2004**, *37*, 5520–5530. (b) Nomura, K.; Fudo, A. *Catal. Commun.* **2003**, *4*, 269–274. (c) Nomura, K.; Komatsu, T.; Imanishi, Y. *Macromolecules* **2000**, *33*, 8122–8124.
(30) (a) Nomura, K.; Oya, K.; Imanishi, Y. *J. Mol. Catal. A: Chem.* **2001**, *174*, 127–140. (b) Nomura, K.; Komatsu, T.; Imanishi, Y. *J. Mol. Catal. A: Chem.* **2000**, *159*, 127–137. (c) Nomura, K.; Komatsu, T.; Imanishi, Y. *J. Mol. Catal. A: Chem.* **2000**, *152*, 249–252. (d) Nomura, K.; Oya, K.; Komatsu, T.; Imanishi, Y. *Macromolecules* **2000**, *33*, 3187–3189.
(31) (a) Nomura, K.; Okumura, H.; Komatsu, T.; Naga, N. *Macromolecules* **2002**, *35*, 5388–5395. (b) Nomura, K.; Okumura, H.; Komatsu, T.; Naga, N.; Imanishi, Y. *J. Mol. Catal. A: Chem.* **2002**, *190*, 225–234.
(32) Wang, W.; Fujiki, M.; Nomura, K. *J. Am. Chem. Soc.* **2005**, *127*, 4582–4583.
(33) (a) Nomura, K.; Tsubota, M.; Fujiki, M. *Macromolecules* **2003**, *36*, 3797–3799. (b) Wang, W.; Tanaka, T.; Tsubota, M.; Fujiki, M.; Yamanaka, S.; Nomura, K. *Adv. Synth. Catal.* **2005**, *347*, 433–446.
(34) Nomura, K.; Liu, J. Y.; Padmanabhan, S.; Kitiyanan, B. *J. Mol. Catal. A: Chem.* **2007**, *267*, 1–29.
(35) Kitiyanan, B.; Nomura, K. *Organometallics* **2007**, *26*, 3461–3465.
(36) Xu, J. S.; Zhang, Y. T.; Li, G. H.; Mu, Y.; Feng, S. H. *Polyhedron* **2006**, *25*, 3071–3076.

Scheme 1. Catalyst Precursor Structures

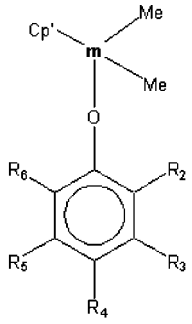

m = Ti, Zr
Cp' = C_5H_5 (Cp), C_5Me_5 (Cp*), $C_5H_3C_6H_4$ (Ind)
R = H, Me, Et, ^{i}Pr, ^{t}Bu, OMe, F, Cl, Br, I, Ph, CH_2Ph, cyclohexyl

(e) change the chain-initiating group. Each of these five variants was studied experimentally and computationally; however, the effects of chain initiating group will be presented in a later paper dealing with chain initiation kinetics. Herein, we focus on the chain propagation kinetics.

Experimental Section

Catalyst Precursor Synthesis. Scheme 1 shows the chemical structure of a mixed Cp′/ArO dimethyl catalyst precursor. The particular precatalysts synthesized are **1**−**24**, **30**, and **31** of Table 1. Extensive precautions were taken to exclude air and moisture and other sources of contamination during catalyst preparation and use. All synthesis and polymerization experiments were carried out using either standard Schlenk line techniques or a circulating nitrogen-filled glovebox operating at less than 0.2 ppm of oxygen. The hydrocarbon solvents were distilled from sodium/benzophenone or purified using an Innovative Technologies solvent purification system and were stored over sodium ribbons under nitrogen until use.

Synthesis details for most of the precatalysts used here were previously reported.[11,23,26,37] In addition, the following new catalyst precursors were synthesized: **20**−**24**, **30**, and **31**. Additional synthesis details for **24** can be found in the thesis by Sharma.[38] The precursors were activated with 1 equiv of $B(C_6F_5)_3$ or $Ph_3CB(C_6F_5)_4$ and used to polymerize 1-hexene. Activation with $B(C_6F_5)_3$ is denoted by adding **a** after the precursor (e.g., **10a**), while activation with $Ph_3CB(C_6F_5)_4$ is denoted by adding **b** after the precursor (e.g., **10b**).

The following measures were taken to ensure that the precatalysts were of acceptable purity. In general, the amounts of LiMe and other chemicals have to be quite exact to get clean products. Care was taken to use a relatively fresh bottle of LiMe so that there could be certainty regarding its concentration and purity. Precatalysts were checked for purity by ^{1}H NMR and elemental analysis before use. The whole batch of precatalyst was discarded and remade if the purity was less than ca. 90% by ^{1}H NMR. All solid precatalysts were stored inside a drybox at room temperature and recrystallized before use. (Microcrystals were grown by placing a concentrated hexane or toluene solution in a freezer overnight.) All liquid precatalysts were stored at −20 °C in a drybox freezer and discarded 2−3 weeks after synthesis.

Cp*Ti(OC$_6$H$_4$-2-Br)Me$_2$ (20). LiMe (3.24 mL, 1.6 M sol. in diethyl ether, 5.18 mmol) was added dropwise to a suspension of Cp^*TiCl_3 (0.500 g, 1.73 mmol) in 30 mL of Et_2O at 0 °C. The mixture was stirred at 0 °C for 1 h and at room temperature for 2 h. The mixture was then cooled back to 0 °C and a solution of 2-bromophenol (0.299 g, 1.73 mmol) in 10 mL of Et_2O was added dropwise. The mixture was slowly warmed to room temperature and was stirred overnight. The solvent was removed under vacuum, and benzene was added to the solid residue. The suspension was filtered through a plug of Celite over fritted glass to remove the lithium salts. The filtrate was then evacuated to dryness, yielding a yellow solid (0.52 g, 78%). Anal. Calcd for $C_{18}H_{25}BrOTi$: C, 56.16; H, 6.49. Found: C, 55.84; H, 6.52. ^{1}H NMR (C_6D_6, 25 °C): δ 7.45 (d, 1H, Ar H); 6.93 (t, 1H, Ar H); 6.85 (d, 1H, Ar H); 6.51 (t, 1H, Ar H); 1.76 (s, 15H, Cp*); 0.86 (s, 6H, Ti−Me). Selected ^{13}C NMR (C_6D_6, 25 °C): δ 161.1 (Ti−O−*C*); 123.0 (*C*$_5$Me$_5$); 57.3 (Ti−-Me); 11.5 (C$_5$*Me*$_5$).

Cp*Ti(OC$_6$H$_4$-2-Ph)Me$_2$ (21). LiMe (3.24 mL, 1.6 M sol. in diethyl ether, 5.18 mmol) was added dropwise to a suspension of Cp^*TiCl_3 (0.500 g, 1.73 mmol) in 30 mL of Et_2O at 0 °C. The mixture was stirred at 0 °C for 1 h and at room temperature for 2 h. The mixture was then cooled back to 0 °C, and a solution of 2-phenylphenol (0.294 g, 1.73 mmol) in 10 mL of Et_2O was added dropwise. The mixture was slowly warmed to room temperature and was stirred overnight. The solvent was removed under vacuum, and benzene was added to the solid residue. The suspension was filtered through a plug of Celite over fritted glass to remove the lithium salts. The filtrate was evacuated to dryness, yielding a yellow solid (0.62 g, 94%). Anal. Calcd for $C_{24}H_{30}OTi$: C, 75.43; H, 7.85. Found: C, 75.68; H, 7.91. ^{1}H NMR (C_6D_6, 25 °C): δ 7.68 (d, 2H, Ar H); 6.90−7.40 (m, Ar H); 1.56 (s, 15H, Cp*); 0.68 (s, 6H, Ti−Me). Selected ^{13}C NMR (C_6D_6, 25 °C): δ 161.9 (Ti−O−*C*); 122.9 (*C*$_5$Me$_5$); 55.7 (Ti−Me); 11.6 (C$_5$*Me*$_5$).

IndTi(OC$_6$H-2,3,5,6-Ph$_4$)Me$_2$ (22). A solution of $IndTiCl_3$ (1.00 g, 3.71 mmol) in 50 mL of dichloromethane was cooled to −78 °C in a dry ice/acetone bath. To this solution was added MeMgBr (3.71 mL, 3.0 *M* in diethyl ether, 11.1 mmol) dropwise via syringe under a flush of nitrogen. After the mixture was stirred for 1 h at −78 °C, a solution of 2,3,5,6-tetraphenylphenol (1.48 g, 3.71 mmol) in dichloromethane was added dropwise. The mixture was slowly warmed to room temperature and stirred for 2 days. The solvent was removed under vacuum, and benzene was added to the solid residue. The suspension was filtered through a plug of Celite over fritted glass to remove magnesium salts. The filtrate was evacuated to dryness, yielding a yellow powder (1.71 g, 78%). Crystals suitable for single-crystal X-ray crystallography were obtained by layering hexane on a benzene solution. Anal. Calcd for $C_{41}H_{34}OTi$: C, 83.42; H, 5.76. Found: C, 83.51; H, 6.11. ^{1}H NMR (C_6D_6, 25 °C): δ 6.80−7.40 (m, Ar H); 5.72 (d, J = 3.0 Hz, 2H, Ind); 5.11 (t, J = 3.0 Hz, 1H, Ind); 0.00 (s, 6H, Ti−Me). Selected ^{13}C NMR (C_6D_6, 25 °C): δ 161.8 (Ti−O−*C*); 116.6, 104.7 (Ind); 61.5 (Ti−*Me*).

IndTi(OC$_6$H$_3$-2,6-^{i}Pr$_2$)Me$_2$ (23). A solution of $IndTiCl_3$ (1.00 g, 3.72 mmol) in 30 mL of dichloromethane was cooled to −78 °C in a dry ice/acetone bath. To this solution was added MeMgCl (3.72 mL, 3.0 *M* in THF, 11.2 mmol) dropwise via syringe under a flush of nitrogen. After the mixture was stirred for 1 h at −78 °C, a solution of 2,6-diisopropylphenol (0.663 g, 3.72 mmol) in dichloromethane was added dropwise. The mixture was slowly warmed to room temperature and stirred for 1 h. The solvent was removed under vacuum, and benzene was added to the solid residue. The suspension was filtered through a plug of Celite over fritted glass to remove magnesium salts. The filtrate was evacuated to dryness, yielding a dark red viscous liquid (1.16 g, 84%). Anal. Calcd for $C_{23}H_{30}OTi$: C, 74.64; H, 8.11. Found: C, 74.15; H, 7.74. ^{1}H NMR (C_6D_6, 25 °C): δ 7.28 (m, 2H, Ind); 7.12 (d, J = 7.8 Hz, 2H, *m*-H); 7.01 (t, J = 7.8 Hz, 1H, *p*-H); 6.89 (m, 2H, Ind); 6.18 (d, J = 3.3 Hz, 2H, Ind); 5.87 (t, J = 3.3 Hz, 1H, Ind); 3.28 (m, J = 6.9 Hz, 2H, C*H*Me$_2$); 1.25 (d, J = 6.9 Hz, 12H, CH*Me*$_2$); 0.67

(37) Fenwick, A. E.; Phomphrai, K.; Thorn, M. G.; Vilardo, J. S.; Trefun, C. A.; Hanna, B.; Fanwick, P. E.; Rothwell, I. P. *Organometallics* **2004**, *23*, 2146–2156.

(38) Sharma, S. Ph.D. Thesis, Chemistry Department, Purdue University, 2005.

Table 1. Computed Ion Pair Separation Energies and Ligand Cone Angles for [Cp′m(OAr)Me]$^+$[A]$^-$ [a]

							SCF E_{IPS} (kcal/mol)				fitted param (kcal/mol)		
precat no.	**m**	Cp′	OAr substituent	[A]$^-$	$\theta_{Cp'}$ (deg)	θ_{OAr} (deg)	vac	C_6H_5-Me	C_6H_5-Br	C_6H_4-1,2-Cl_2	B	C	rms err
1	Ti	Cp	2,6-Me_2-4-Br	[$MeBQ_3$]$^-$	128	129	74.01	35.74	19.65	13.70	7.23	66.92	0.2
2	Ti	Cp	2,6-Et_2	[$MeBQ_3$]$^-$	129	132	72.16	34.63	18.75	12.94	6.59	65.72	0.3
3	Ti	Cp	2,6-^{i}Pr$_2$	[$MeBQ_3$]$^-$	130	136	69.83	34.07	19.27	13.90	7.76	62.13	0.1
4	Ti	Cp*	none	[$MeBQ_3$]$^-$	155	96	66.02	31.42	16.98	11.69	5.80	60.32	0.2
5	Ti	Cp*	4-F	[$MeBQ_3$]$^-$	156	96	67.10	32.08	17.81	12.49	6.51	60.63	0.1
6	Ti	Cp*	4-Cl	[$MeBQ_3$]$^-$	156	96	67.06	32.09	17.80	12.47	6.50	60.60	0.1
7	Ti	Cp*	4-Br	[$MeBQ_3$]$^-$	156	96	67.06	31.80	17.15	11.75	5.75	61.40	0.2
8	Ti	Cp*	4-Ph	[$MeBQ_3$]$^-$	156	96	65.27	31.20	17.04	11.84	6.03	59.32	0.1
9	Ti	Cp*	4-^{t}Bu	[$MeBQ_3$]$^-$	156	95	64.70	30.95	16.67	11.40	5.71	59.13	0.2
10	Ti	Cp*	2,6-Me_2	[$MeBQ_3$]$^-$	154	127	62.00	28.88	15.37	10.52	4.78	57.24	0.0
				[BQ_4]$^-$	158	130	52.24	23.38	12.15	8.18	3.05	49.08	0.2
11	Ti	Cp*	2,6-Et_2	[$MeBQ_3$]$^-$	155	132	61.26	28.39	14.86	9.98	4.31	56.99	0.1
				[BQ_4]$^-$	158	140	51.44	22.71	11.41	7.40	2.32	49.04	0.1
12	Ti	Cp*	2,6-^{i}Pr$_2$	[$MeBQ_3$]$^-$	154	136	59.53	26.64	13.42	8.69	2.95	56.56	0.0
				[BQ_4]$^-$	159	138	50.67	22.34	11.33	7.46	2.41	48.14	0.2
13	Ti	Cp*	2-cyclohexyl	[$MeBQ_3$]$^-$	155[d]	125[d]	63.56[d]	30.17[d]	16.71[d]	11.88[d]	6.06[d]	57.48[d]	0.0[d]
					156[p]	127[p]	64.89[p]	30.91[p]	16.95[p]	11.85[p]	6.02[p]	58.92[p]	0.1[p]
14	Ti	Cp*	2,6-Me_2-4-Br	[$MeBQ_3$]$^-$	155	127	63.25	29.61	15.72	10.70	4.91	58.39	0.1
15	Ti	Cp*	2-CH_2Ph	[$MeBQ_3$]$^-$	155[d]	113[d]	57.30[d]	23.86[d]	10.57[d]	5.85[d]	−0.03[d]	57.27[d]	0.1[d]
					156[p]	111[p]	65.46[p]	31.10[p]	16.86[p]	11.63[p]	5.77[p]	59.77[p]	0.1[p]
16	Ti	Cp*	2,3,5,6-Ph_4	[$MeBQ_3$]$^-$	154	163	46.57	14.06	0.78	−4.04	−9.65	56.24	0.0
17	Ti	Cp*	3-OMe	[$MeBQ_3$]$^-$	156[d]	96[d]	65.14[d]	30.72[d]	16.48[d]	11.24[d]	5.37[d]	59.85[d]	0.1[d]
					155[p]	96[p]	65.19[p]	31.06[p]	18.17[p]	11.80[p]	6.51[p]	58.70[p]	0.5[p]
18	Ti	Cp*	4-OMe	[$MeBQ_3$]$^-$	156	96	63.75	30.24	16.17	10.98	5.31	58.56	0.2
19	Ti	Cp	2,3,5,6-Ph_4	[$MeBQ_3$]$^-$	130	167	55.19	20.89	6.70	1.54	−4.34	59.60	0.1
				[BQ_4]$^-$	130	188	45.72	17.12	5.76	1.71	−3.32	48.98	0.1
20	Ti	Cp*	2-Br	[$MeBQ_3$]$^-$	154[d]	118[d]	56.88[d]	23.63[d]	9.66[d]	4.87[d]	−0.93[d]	57.88[d]	0.1[d]
					155[p]	117[p]	57.70[p]	24.19[p]	10.65[p]	5.82[p]	−0.03[p]	57.72[p]	0.0[p]
21	Ti	Cp*	2-Ph	[$MeBQ_3$]$^-$	154[d]	127[d]	59.23[d]	25.36[d]	11.78[d]	6.92[d]	1.00[d]	58.20[d]	0.1[d]
					154[p]	128[p]	59.54[p]	26.02[p]	12.59[p]	7.78[p]	1.92[p]	57.59[p]	0.1[p]
22	Ti	Ind	2,3,5,6-Ph_4	[$MeBQ_3$]$^-$	136	169	53.04	19.61	5.80	0.75	−4.97	58.07	0.1
23	Ti	Ind	2,6-^{i}Pr$_2$	[$MeBQ_3$]$^-$	136	138	63.99	28.97	14.68	9.52	3.46	60.55	0.0
24	Zr	Cp*	2,3,5,6-Ph_4	[$MeBQ_3$]$^-$	149	155	53.26	20.21	6.43	1.36	−4.26	57.61	0.2
25	Zr	Cp*	2,6-^{i}Pr$_2$	[$MeBQ_3$]$^-$	149	134	69.73	36.25	22.60	17.66	11.87	57.88	0.0
				[BQ_4]$^-$	151	133	57.38	27.81	16.03	11.83	6.64	50.69	0.1
26	Ti	Cp*	2-F	[$MeBQ_3$]$^-$	156[d]	105[d]	63.22[d]	29.92[d]	16.54[d]	11.78[d]	5.95[d]	57.24[d]	0.1[d]
					155[p]	105[p]	63.36[p]	29.63[p]	15.97[p]	11.09[p]	5.21[p]	58.14[p]	0.0[p]
27	Ti	Cp*	2-Cl	[$MeBQ_3$]$^-$	155[d]	114[d]	59.22[d]	26.03[d]	12.63[d]	7.86[d]	2.06[d]	57.13[d]	0.0[d]
					155[p]	114[p]	60.06[p]	26.09[p]	12.53[p]	7.69[p]	1.74[p]	58.27[p]	0.1[p]
28	Ti	Cp*	2-I	[$MeBQ_3$]$^-$	154[d]	120[d]	53.37[d]	20.26[d]	6.85[d]	2.08[d]	−3.70[d]	57.06[d]	0.0[d]
					156[p]	120[p]	54.51[p]	21.04[p]	7.48[p]	2.62[p]	−3.20[p]	57.71[p]	0.0[p]
29	Ti	Cp*	4-I	[$MeBQ_3$]$^-$	155	96	64.66	29.79	15.10	9.68	3.79	61.01	0.2
30	Ti	Cp*	2,6-$(OMe)_2$	[$MeBQ_3$]$^-$	155	135	53.70	21.26	7.95	3.18	−2.43	56.16	0.1
31	Ti	Cp*	2,6-^{i}Pr$_2$-4-Br	[$MeBQ_3$]$^-$	154	135	61.12	27.92	14.47	9.64	3.87	57.25	0.0

[a] Legend: d, aryloxide substituent distal to initiating group; p, aryloxide substituent proximal to initiating group. Q = C_6F_5.

(s, 6H, Ti−Me). ^{13}C NMR (C_6D_6, 25 °C): δ 161.6 (Ti−O−*C*); 138.6, 127.0, 125.9, 125.7, 123.8, 122.9 (aromatics); 117.3, 104.6 (Ind); 58.2 (Ti−*Me*); 27.6 (*C*HMe$_2$); 24.1 (CH*Me*$_2$).

Cp*Zr(OC$_6$H-2,3,5,6-Ph$_4$)Cl$_2$. A sample of Li(OC$_6$H-2,3,5,6-Ph$_4$)·Et$_2$O (0.65 g, 1.36 mmol) was added to a suspension containing Cp*ZrCl$_3$ (0.45 g, 1.35 mmol) in 50 mL of benzene. The resulting solution was stirred at room temperature overnight and filtered through a plug of Celite over fritted glass to remove LiCl. The solvent was removed under vacuum to give a white solid (0.86 g, 91%). A small amount of this solid (20 mg) was dissolved in a minimum amount of hot benzene and layered with hexane, affording white crystals of Cp*Zr(OC$_6$H-2,3,5,6-Ph$_4$)Cl$_2$ as a benzene solvate (11 mg, 55%). Anal. Calcd for $C_{40}H_{36}OZrCl_2$: C, 69.15; H, 5.22. Found: C, 69.87; H, 5.64. ^{1}H NMR (C_6D_6, 25 °C): δ 6.90−7.40 (aromatics); 1.53 (s, 15H, Cp*). Selected ^{13}C NMR (C_6D_6, 25 °C): δ 179.1 (Zr−O−C); 126.3 (Cp*); 11.0 (*Me*, Cp*).

Cp*Zr(OC$_6$H-2,3,5,6-Ph$_4$)Me$_2$ (24). A diethyl ether solution of Cp*Zr(OC$_6$H-2,3,5,6-Ph$_4$)Cl$_2$ (0.3 g, 0.43 mmol) was cooled to 0 °C in an ice bath. To this solution was added MeLi·LiBr (0.57 mL, 0.86 mmol) via syringe under a flush of nitrogen. The solution was stirred at 0 °C in ice bath for an additional 3 h, and the solvent was removed under vacuum and replaced with benzene. The suspension was filtered through a plug of Celite over fritted glass to remove lithium salts. The filtrate was evacuated to afford a white solid (0.21 g, 74%). The solid (22 mg) was dissolved in a minimum amount of hot benzene, and this solution was layered with hexane and allowed to sit overnight to give white needle-shaped crystals of the title compound as a benzene solvate (15 mg, 68%). Anal. Calcd for $C_{42}H_{42}OZr$. C_6H_6: C, 78.75; H, 6.61. Found: C, 78.44; H, 6.50. ^{1}H NMR (C_6D_6, 25 °C): δ 6.90−7.40 (aromatics); 1.53 (s, 15H, C_5*Me*$_5$); −0.13 (s, 6H, Zr−*Me*). Selected ^{13}C NMR (C_6D_6, 25 °C): δ 158.1 (Zr−O−C); 120.0 (C_5Me$_5$); 42.7 (Zr−*Me*), 11.1 (C_5*Me*$_5$).

Cp*Ti(OC$_6$H$_3$-2,6-(OMe)$_2$)Me$_2$ (30). LiMe (3.24 mL, 1.6 M solution in diethyl ether, 5.18 mmol) was added dropwise to a suspension of Cp*TiCl$_3$ (0.500 g, 1.73 mmol) in 30 mL of Et$_2$O at 0 °C. The mixture was stirred at 0 °C for 1 h and at room temperature for 2 h. The mixture was then cooled back to 0 °C, and a solution of 2,6-dimethoxyphenol (0.266 g, 1.73 mmol) in 10 mL of Et$_2$O was added dropwise. The mixture was slowly warmed to room temperature and stirred overnight. The solvent was removed under vacuum, and benzene was added to the solid residue. The suspension was filtered through a plug of Celite over fritted glass to remove lithium salts. The filtrate was evacuated to dryness, yielding a yellow liquid (0.52 g, 82%). Anal. Calcd for $C_{20}H_{30}O_3Ti$: C, 65.62; H, 8.19. Found: C, 65.45; H, 8.02. ^{1}H NMR (C_6D_6, 25 °C): δ 7.76 (t, J = 8.1 Hz, 1H, *p*-H); 6.43 (d, J = 8.4 Hz, 2H, *m*-H); 3.42 (s, 6H, OMe); 1.86 (s, 15H, Cp*); 0.89 (s, 6H, Ti−Me).

^{13}C NMR (C_6D_6, 25 °C): δ 152.0 (Ti−O−*C*); 145.1, 119.8, 106.0 (aromatics); 122.6 (*C*$_5$Me$_5$); 55.9 (OMe); 55.0 (Ti−Me); 11.7 (C$_5$*Me*$_5$).

Cp*Ti(OC$_6$H$_2$-2,6-^{i}Pr$_2$-4-Br)Me$_2$ (31). LiMe (3.24 mL, 1.6 M solution in diethyl ether, 5.18 mmol) was added dropwise to a suspension of Cp*TiCl$_3$ (0.500 g, 1.73 mmol) in 30 mL of Et$_2$O at 0 °C. The mixture was stirred at 0 °C for 1 h and at room temperature for 2 h. The mixture was then cooled back to 0 °C, and a solution of 4-bromo-2,6-diisopropylphenol (0.445 g, 1.73 mmol) in 10 mL of Et$_2$O was added dropwise. The mixture was slowly warmed to room temperature and was stirred overnight. The solvent was removed under vacuum, and benzene was added to the solid residue. The suspension was filtered through a plug of Celite over fritted glass to remove lithium salts. The filtrate was evacuated to dryness, yielding an orange solid (0.75 g, 92%). X-ray-quality crystals were obtained by placing a concentrated hexanes solution in a freezer. Anal. Calcd for $C_{24}H_{37}BrOTi$: C, 61.46; H, 7.89. Found: C, 61.26; H, 8.02. ^{1}H NMR (C_6D_6, 25 °C): δ 7.40 (s, 2H, *m*-H); 3.06 (m, J = 6.9 Hz, 2H, C*H*Me$_2$); 1.68 (s, 15H, Cp*); 1.14 (d, J = 6.9 Hz, 12H, CH*Me*$_2$); 0.70 (s, 6H, Ti−Me). ^{13}C NMR (C_6D_6, 25 °C): δ 158.1 (Ti−O−*C*); 141.3, 127.0, 115.1 (aromatics); 123.0 (*C*$_5$Me$_5$); 55.4 (Ti−Me); 27.5 (*C*HMe$_2$); 23.9 (CH*Me*$_2$); 11.8 (C$_5$*Me*$_5$).

1-Hexene Polymerization Reactions. 1-Hexene polymerization reactions were followed by measuring monomer consumption versus time using ^{1}H NMR or by weighing dried polymer samples at regular intervals of time during the polymerization reaction to compute yields. The polymer samples were purified by extracting into THF and passing the extracts through a short plug of alumina to remove the catalyst. Molecular weight distributions were measured using a Waters Alliance GPCV 2000. Experimental details and data analysis are given in the Supporting Information.

A representative procedure is provided here for the 200:1 monomer−catalyst trial at 0 °C. A solution of precatalyst **13** in toluene-d_8 (25.0 μL, 0.10 M, 2.5 μmol) was added to a mixture of 1-hexene (62.5 μL, 0.500 mmol) and internal standard Ph$_2$CH$_2$ (10 μL) in 0.39 mL of toluene-d_8 in a screw-cap NMR tube with a PTFE/silicone septum. This solution was cooled to 0 °C using a cooler attached to the NMR spectrometer, and an NMR spectrum was taken. A solution of B(C$_6$F$_5$)$_3$ activator in toluene-d_8 (25.0 μL, 0.10 M, 2.5 μmol) was then added through the septum at 0 °C. The NMR tube was shaken vigorously and quickly placed back into the spectrometer. The conversion of 1-hexene was monitored by integrating the proton signal in the olefinic region versus the internal standard Ph$_2$CH$_2$. After the polymerization proceeded to over 95% completion, the solution was poured into excess methanol to precipitate the polymer. The excess methanol was decanted, and the polymer was dried under vacuum overnight.

Computational Methods. To compute ion pair separation energies (E_{IPS}), the geometries of the contact ion pair, bare cation, and bare counterion were first optimized under vacuum using Gaussian 03. The GDIIS method was used to optimize ground-state geometries to better than 0.005 Å for the atom displacements, 0.0025 au for the forces, and 0.02 kcal/mol for the total energies. Several initial conditions were explored whenever there was any doubt about which catalyst conformation had the lowest energy. Once the geometries converged, the lowest energy conformation was utilized.

Once the vacuum geometries were determined, single-point calculations were performed using the polarization continuum model (PCM) to obtain the self-consistent field (SCF) energies in solution. PCM calculations were performed in Gaussian 03 using the default solute cavity generation parameters (UA0 radii).[39] Vacuum geometry optimization was used, because solvent-phase geometry optimization is too computationally expensive. In order to assess the validity of this approach, PCM-geometry optimization was performed for catalysts **1a** and **3a** in a toluene-like solvent, which gave E_{IPS} values within 0.6 kcal/mol of the vacuum-optimized geometries. The computational approach used here was found to give E_{IPS} values that correlate well to experimental reactivity trends.[11]

(39) Frisch, M. J., et al. Gaussian 03, Revision C.02; Gaussian, Inc., Wallingford, CT, 2004.

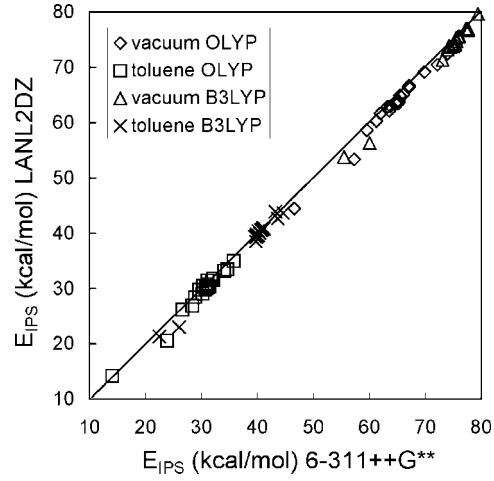

Figure 2. Effect of basis set on computed E_{IPS} values for catalysts **1a**−**18a**. The solid line is $y = x$.

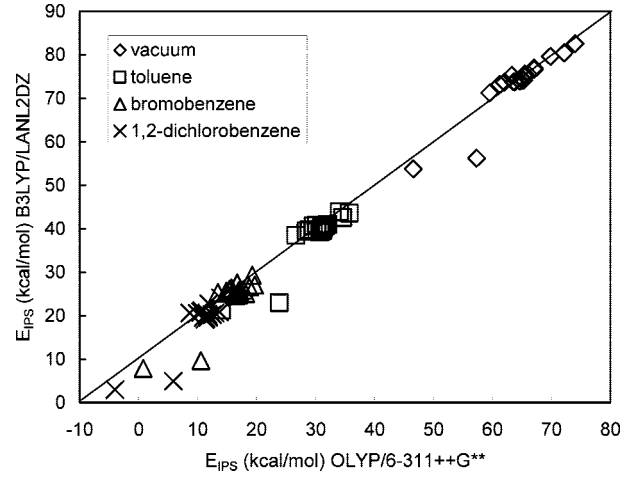

Figure 3. Effect of exchange-correlation functional on computed E_{IPS} values for catalysts **1a**−**18a**. The solid line is $y = x + 10$.

6-311++G** basis sets were used on all atoms, except for I and Zr, which used the Stuttgart/Dresden (SDD) triple-ζ basis set with effective core potentials. This basis set was sufficiently large that basis set superposition error and size limitations could be neglected. The counterpoise correction (which is widely used but known to usually overestimate BSSE) was found to be approximately 2 kcal/mol for the vacuum E_{IPS} value of catalyst **1a** using the OLYP/6−311++G** method. As shown in Figure 2, for catalysts **1a**−**18a** the 6-311++G** E_{IPS} values for vacuum or toluene were 1 (average) ± 1 (standard deviation) kcal/mol higher than the LANL2DZ values, irrespective of the exchange-correlation functional. These results show that basis set size limitations were not appreciable in the calculation of E_{IPS}. The OLYP exchange-correlation functional was used because it afforded reliable performance at reasonable computational cost. Comparisons were made to the more computationally expensive B3LYP functional for catalysts **1a**−**18a** in a series of solvents. As shown in Figure 3, the B3LYP E_{IPS} values were 10 (average) ± 2 (standard deviation) kcal/mol higher than the OLYP values irrespective of the solvent.

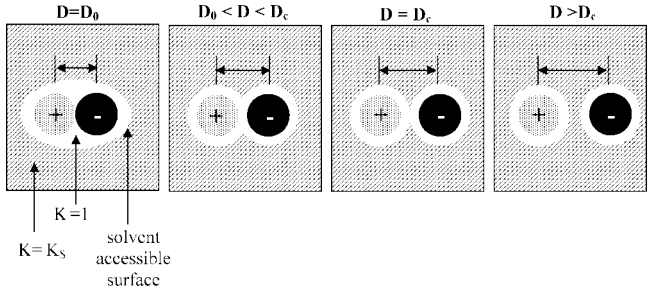

Figure 4. Process of ion pair separation.

These results show E_{IPS} values computed using different exchange-correlation functionals and/or basis sets are linearly correlated to each other.

Results of Experimental and DFT Studies

Ion Pair Separation Energies and Ligand Cone Angles. Figure 4 illustrates the process of ion pair separation. In the ISIP, also called the contact ion pair, the cation and counterion are in direct contact with no solvent in between. Inside the solvent-accessible surface the dielectric constant felt by the ion pair is equal to 1, whereas outside the solvent-accessible surface the dielectric constant felt by the ion pair is equal to the solvent dielectric constant K_S. The charge separation distance between the cation and counterion is denoted as D, where D_0 is the charge separation distance in the contact ion pair. If the counterion is displaced by a very small amount, i.e. by $D_0 < D < D_c$, there is not enough room for a solvent molecule between the cation and counterion. At some critical charge separation distance, D_c, the solvent-accessible surfaces of the cation and counterion touch at a single point. For $D > D_c$, the solvent-accessible surfaces of the cation and counterion are separated by a layer of solvent.

An ion pair separation energy descriptor is needed that measures the intrinsic difficulty of separating the cation from the anion while allowing the cation and anion geometries to relax. In order to have the most utility, the ion pair separation energy descriptor should scale in predictable ways with K_S and D. Using electrostatic arguments to derive scaling relationships, a reliable prediction will be made (see eq 3) of how the *electronic* ion pair separation energy of the system changes with K_S. The "thermodynamic" energies (vibrational, translational, rotational) do not follow this scaling relationship; thus, it is important for the E_{IPS} descriptor to exclude them. The electronic ion pair separation energy, E_{IPS}, is defined as the SCF energy of the isolated cation plus the SCF energy of the isolated counterion minus the SCF energy of the contact ion pair—all computed in the dielectric medium of interest.

What type of scaling relationship should be followed by E_{IPS} as the solvent dielectric constant K_S is changed? When no solvent is present, $K_S = 1$ and E_{IPS} is at its maximum value, and as K_S approaches infinity, E_{IPS} will be at its mimimum value. Because solvent does not penetrate between the cation and counterion in the contact ion pair, some energy B is required to separate them even as K_S approaches infinity:

$$\lim_{K_S \to \infty} E_{IPS} = B \tag{1}$$

In general, E_{IPS} has two parts: (a) the part that is screened by solvent and (b) the part that is not screened by solvent. The part not screened by solvent is equal to B, since no matter how much we increase K_S the energy B remains constant. The fraction of E_{IPS} screened by solvent is equal to the difference between the maximum at $K_S = 1$, as determined from the vacuum energy and the minimum as K_S approaches infinity: specifically

$$C = E_{IPS}[\text{vacuum}] - B \tag{2}$$

From Coulomb's law, the solvent-dependent E_{IPS} portion must be inversely proportional to K_S; thus

$$E_{IPS}[\text{solvent}] = B + C/K_S = C\left(\frac{1}{K_S} - 1\right) + E_{IPS}[\text{vacuum}] \tag{3}$$

where each catalyst has its own B and C values. Once the constants B and C are determined, the E_{IPS} value for that catalyst in different organic solvents can be estimated.

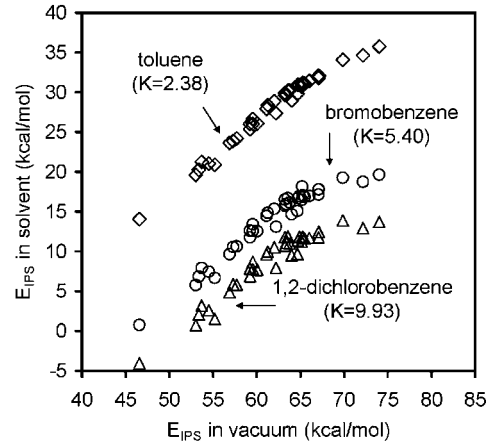

Figure 5. SCF E_{IPS} values in toluene ($K_S = 2.38$), bromobenzene ($K_S = 5.40$), and 1,2-dichlorobenzene ($K_S = 9.93$) for the 29 Cp′Ti(OAr)Me_2/B(C_6F_5)$_3$ catalysts in Table 1.

Activation with B(C_6F_5)$_3$ was studied for a series of 31 catalyst precursors (Table 1). Activation with $Ph_3CB(C_6F_5)_4$ was studied for 5 of these catalyst precursors. In each case, the PCM model was used to compute E_{IPS} values in vacuum, toluene ($K_S = 2.38$), bromobenzene ($K_S = 5.40$), and 1,2-dichlorobenzene ($K_S = 9.93$). Results for the 29 Cp′Ti(OAr)Me_2/B(C_6F_5)$_3$ systems are plotted in Figure 5. For a given catalyst, the value of E_{IPS} decreases as K_S increases. For a given metal and counterion, the value of E_{IPS} in a particular solvent decreases as E_{IPS} in vacuum decreases. A least-squares fit of eq 3 to these E_{IPS} values was performed to obtain the optimized B and C parameters for each catalyst conformation (Table 1). The rms error between eq 3 and the DFT-computed E_{IPS} values was less than 0.5 kcal/mol for each of the catalysts, indicating that eq 3 is the proper functional form.

There are several factors that influence the values of B and C. For a given catalyst precursor, the E_{IPS}, B, and C values are slightly smaller for $[B(C_6F_5)_4]^-$ than for $[MeB(C_6F_5)_3]^-$, reflecting the fact that $[B(C_6F_5)_4]^-$ is more weakly bound than $[MeB(C_6F_5)_3]^-$. This decrease in E_{IPS} is partially due to the slightly larger size of $[B(C_6F_5)_4]^-$, which leads to a larger initial separation distance. For example, the Ti−B distance is 6.65 Å in **12b** compared to 4.19 Å in **12a**. The B and C values tend to decrease as the electron-donating ability of the ligand increases. Specifically, the electron-donating abilities of the cyclopentadienyl ligands follow the order Cp* > Ind > Cp, and for a given aryloxide ligand the B and C values follow the order Cp > Ind > Cp*. In a similar manner, for the aryloxide ligand both B and C decrease with the addition of electron-donating substituents such as Me, Et, ^{i}Pr, etc. On the other hand, addition

Table 2. Effects of Counterion on Activity for $[Cp^*Ti(OC_6H_3\text{-}2,6\text{-}R_2)Me]^+[A]^-$[a]

							$[B(C_6F_5)_4]^-$ to $[MeB(C_6F_5)_3]^-$ activity ratio		
R	$[A]^-$	E_{IPS}(toluene) (kcal/mol)	monomer ratio	t_{quench} (min)	yield (%)	activity (g/(mmol h))	exptl	prediction[b]	adjusted[c]
Me	$[MeB(C_6F_5)_3]^-$	28.9	2000:1	20	55	280	≥24	16	35
	$[B(C_6F_5)_4]^-$	23.9	2000:1	10	100	high			
	$[B(C_6F_5)_4]^-$	23.9	4000:1	3	100	≥6720			
Et	$[MeB(C_6F_5)_3]^-$	28.4	2000:1	20	14	71.4	49	23	51
	$[B(C_6F_5)_4]^-$	22.7	2000:1	10	100	high			
	$[B(C_6F_5)_4]^-$	22.7	4000:1	3	52	3500			
^{i}Pr	$[MeB(C_6F_5)_3]^-$	26.6	2000:1	20	3.7	18.6	22−30	11	24
	$[B(C_6F_5)_4]^-$	22.3	2000:1	10	40	404			
	$[B(C_6F_5)_4]^-$	22.3	4000:1	3	8	552			

[a] Reactions at 25 °C with 2.0 M 1-hexene in toluene solvent. [b] Prediction based upon change in E_{IPS} assuming A, α, and f are the same for both counterions. [c] Based upon change in E_{IPS} assuming α and f are the same for both counterions and A is 2.2 times larger for $[B(C_6F_5)_4]^-$ than for $[MeB(C_6F_5)_3]^-$.

of electron-withdrawing groups such as F, Cl, Br, and I in the para position increases B and C. As reflected by the B and C values, for a given ligand structure it is much harder to separate the $[MeB(C_6F_5)_3]^-$ counterion from a Zr catalyst than from the corresponding Ti catalyst. Surprisingly, some of the catalysts have negative B values, which implies that the global ground state of these catalysts as K_S approaches infinity is an SSIP. This unusual behavior is due to opportunistic coordination of the ligand upon ion pair separation, as explained in the next section.

Also shown in Table 1 are the computed ligand cone angles for each of the catalyst systems. The ligand cone angle, θ_{lig}, was defined as the largest X−**m**−Y angle, where **m** is the center of the metal atom and X and Y are two points on the van der Waals surface of the ligand outside the metal's van der Waals sphere. θ_{lig} lies between the angle θ_{max} of a circular cone (with the apex at the metal center) that completely encompasses the ligand's van der Waals surface and the angle $\theta_{min} = 2\ \mathrm{acos}[1 - \Omega/(2\pi)]$ of a circular cone that subtends a solid angle equal to the solid angle Ω subtended by the ligand's van der Waals surface:[40]

$$\theta_{min} \le \theta_{lig} \le \theta_{max} \quad (4)$$

The predicted solid angle ($\Omega_{lig} = 4\pi \sin^2(\theta_{lig}/4)$) blocked by the ligand lies between the actual solid angle Ω subtended by the ligand's van der Waals surface and the solid angle subtended by the circular cone of angle θ_{max}. Because the van der Waals surface of the ligand may contain inaccessible crevices, one expects the true measure of solid angle blocked by the ligand to satisfy the same bounds.

The cone angles reveal that the Ind ligand (136°) is more sterically hindering than the Cp ligand (∼129°) but less sterically hindering than the Cp* ligand (∼155°). There is a very large difference in steric hindrance between catalysts with zero, one, or two ortho substituents on the aryloxide ligand. For the Ti catalysts, we note that θ_{OAr} varies from 95 to 96° for no ortho substituents, from 105 to 128° for one ortho substituent, and from 127 to 188° for two ortho substituents. Also, a ligand on Zr is slightly less sterically hindering than the same ligand on Ti, because the larger diameter of Zr causes the ligand to be located slightly farther from the metal center, which in turn decreases the ligand cone angle. In summary, the degree of steric hindrance at the metal center is primarily determined by (i) the type of cyclopentadienyl ring (i.e., Cp, Ind, or Cp*), (ii) the number of ortho substituents on the aryloxide ring, and (iii) the metal. The growing polymer chain also contributes to steric hindrance at the metal center.

Table 2 compares the activity of catalysts **10**−**12** activated with $B(C_6F_5)_3$ and $Ph_3CB(C_6F_5)_4$. For each of these catalysts, the activity for the $[B(C_6F_5)_4]^-$ counterion was higher than for the $[MeB(C_6F_5)_3]^-$ counterion. The increase in activity can be attributed to the lower E_{IPS} value for $[B(C_6F_5)_4]^-$ compared to that for the $[MeB(C_6F_5)_3]^-$ counterion.

Opportunistic Coordination of Some Ortho Substituents to the Metal Center. On examination of the data in Table 1, some catalysts have comparatively low B values, which we postulate is caused by opportunistic coordination of a ligand substituent to the metal upon ion separation. The formation of this partial bond between the metal and ligand substituent in the bare cation lowers the energy required to separate the ion pair. The parameter B becomes negative when the energy gain from the formation of this partial bond exceeds the energy required to break the cation−counterion bond as K_S approaches infinity. To quantify these effects, selected geometric parameters and bond orders were computed for each catalyst.

For all of the contact ion pairs in Table 3, the Ti−O−Ar bond angle is nearly straight (163.7−178.0°). For the cations, about half of the structures (group 1) have a Ti−O−Ar bond angle in the range of 172.6−177.7°, while the other half (group 2, boldface) lie in the range of 122.8−151.3°. The bending of the Ti−O−Ar angle in the cations of group 2 allows the ortho substituent to move closer to and form a partial bond with the metal. Figure 6 shows the geometries of the proximal and distal cations and ion pairs for catalyst **20a**. One can clearly see that the Ti−O−Ar bond angle is nearly straight in the contact ion pairs but substantially bent in the bare cations.

The Wiberg bond index array was computed using natural bond orbital (NBO) analysis in the Gaussian 03 program. The Wiberg bond index array is a measure of the effective bond order between atoms in a molecular structure.[41] The largest partial bond orders between any ortho substitutent group atom and the metal center are given in the last two columns of Table 3. For all of the contact ion pairs and the cations in group 1 the effective bond order was 0, implying there was no bonding between the ortho substituent group and the metal center.

(40) Consider the solid angle Ω of the shadow cast when a point source of light is placed at the metal center **m** by the portion of the ligand's van der Waals surface lying outside the metal's van der Waals radius onto a sphere surrounding the ligand. Among all surfaces that subtend a solid angle Ω, the circular cone has the smallest maximum angle X−**m**−Y (aka θ_{min}), where X and Y are any two points on the surface; therefore, the maximum X−**m**−Y angle of the ligand's van der Waals surface (aka θ_{lig}) must be greater than or equal to θ_{min}. The maximum angle X−**m**−Y of the ligand's van der Waals surface (i.e. θ_{lig}) lies on the surface of the circular cone (with apex at the metal center) completely enclosing the ligand's van der Waals surface; therefore, the angle θ_{max} across this cone must necessarily be greater than or equal to θ_{lig}.

(41) Wiberg, K. B. *Tetrahedron* **1968**, *24*, 1083–1096.

Table 3. Properties of Selected [Cp*Ti(OAr)Me]$^+$[MeB(C$_6$F$_5$)$_3$]$^-$[a]

				Ti−O−Ar (deg)		Ti−X dist[b] (Å)		Ti−X Wiberg bond index[b,c]	
OAr substituent	E_{IPS}(toluene) (kcal/mol)	*A* (kcal/mol)	*B* (kcal/mol)	cation	IP	cation	IP	cation	IP
none (X = H)	31.42	60.32	5.80	175.6	174.4	3.94	3.94	0.0	0.0
2-F	29.92[d]	57.24[d]	5.95[d]	**125.8**[d]	175.8[d]	**2.32**[d]	3.96[d]	**0.2**[d]	0.0[d]
	29.63[p]	58.14[p]	5.21[p]	**126.0**[p]	172.7[p]	**2.33**[p]	3.99[p]	**0.2**[p]	0.0[p]
4-F	32.08	60.63	6.51	176.4	174.6	7.26	7.28	0.0	0.0
2-Cl	26.03[d]	57.24[d]	5.95[d]	**135.3**[d]	170.9[d]	**2.67**[d]	4.27[d]	**0.4**[d]	0.0[d]
	26.09[p]	58.14[p]	5.21[p]	**135.3**[p]	170.2[p]	**2.67**[p]	4.26[p]	**0.4**[p]	0.0[p]
4-Cl	32.09	60.60	6.50	176.6	173.7	7.69	7.67	0.0	0.0
2-Br	23.63[d]	57.88[d]	−0.93[d]	**138.5**[d]	170.0[d]	**2.78**[d]	4.63[d]	**0.5**[d]	0.0[d]
	24.19[p]	57.72[p]	−0.03[p]	**138.3**[p]	167.7[p]	**2.78**[p]	4.41[p]	**0.5**[p]	0.0[p]
4-Br	31.80	61.40	5.75	177.3	173.6	7.84	7.85	0.0	0.0
2-I	20.26[d]	57.06[d]	−3.70[d]	**144.3**[d]	166.8[d]	**3.00**[d]	4.57[d]	**0.6**[d]	0.0[d]
	21.04[p]	57.71[p]	−3.20[p]	**143.7**[p]	166.6[p]	**2.99**[p]	4.56[p]	**0.6**[p]	0.0[p]
4-I	29.79	61.01	3.79	175.0	174.7	8.07	8.08	0.0	0.0
2-Ph	25.36[d]	58.20[d]	1.00[d]	**148.9**[d]	163.7[d]	**2.62**[d]	4.17[d]	**0.2**[d]	0.0[d]
	26.02[p]	57.59[p]	1.92[p]	**146.5**[p]	164.4[p]	**2.50**[p]	4.31[p]	**0.2**[p]	0.0[p]
4-Ph	31.20	59.32	6.03	177.7	175.1	7.46	7.46	0.0	0.0
2-cyclohexyl	30.17[d]	57.48[d]	6.06[d]	174.6[d]	164.2[d]	3.21[d]	3.61[d]	0.0[d]	0.0[d]
	30.91[p]	58.92[p]	6.02[p]	172.6[p]	166.2[p]	3.34[p]	3.50[p]	0.0[p]	0.0[p]
2,3,5,6-Ph$_4$	14.06	56.24	−9.65	**151.3**	178.0	**2.67**	4.07	**0.2**	0.0
2,6-(OMe)$_2$	21.26	56.16	−2.43	**122.8**	173.4	**2.22**	3.83	**0.2**	0.0

[a] Legend: d, aryloxide substituent distal to initiating group; p, aryloxide substituent proximal to initiating group. [b] The smallest Ti−X distance and largest Ti−X bond index for any atom in the OAr substituent. [c] In toluene-like solvent computed using natural bond orbital analysis.

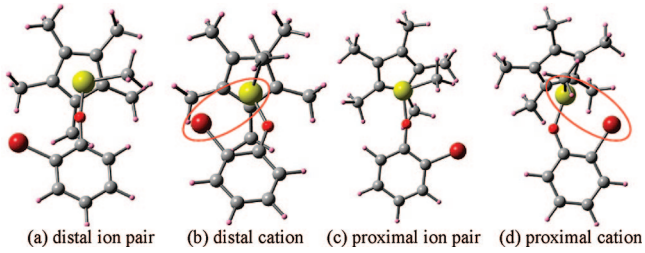

Figure 6. [Cp*Ti(OC$_6$H$_4$-2-Br)Me]$^+$ geometry in the (a) distal contact ion pair, (b) distal bare cation, (c) proximal contact ion pair, and (d) proximal bare cation. For clarity, the [MeB(C$_6$F$_5$)$_3$]$^-$ counterion is not shown in the ion pairs.

However, for all the cations in group 2 there was clear evidence for the formation of a partial bond between the ortho substituent and the metal center, where the computed effective bond order ranged from 0.2 to 0.6.

The Ti−X distance was taken to be the distance between the Ti center and the closest ortho substituent group atom. For catalysts in group 1, the Ti−X distance was similar for the cation and ion pair. For catalysts in group 2, the Ti−X distance was substantially shorter in the cation than in the ion pair, due to the formation of a partial Ti−X bond in the cation.

In addition to the catalysts **16a**, **20a**, **28a**, and **30a** discussed above, Table 1 shows that the Cp (**19a**,**b**), Ind (**22a**), and Zr (**24a**) analogues of **16a** also have negative *B* values. For these complexes, the bare cations have **m**−O−Ar angles smaller than 150° and display partial coordination between the ortho substituent and metal center.[42] These results show that opportunistic ligand coordination occurs irrespective of the type of metal (Ti or Zr), counterion, and ancillary Cp′ ligand (Cp, Ind, or Cp*).

There is a simple chemical explanation for the occurrence of opportunistic ligand bonding in catalysts **16**, **19**−**22**, **24**, **26**−**28**, and **30** activated with either counterion. The positively charged metal prefers a four-coordinate pseudotetrahedral environment. In the ion pair, these four sites are filled by (i) the cyclopentadienyl ligand, (ii) the aryloxide ligand, (iii) the initiating group or growing chain, and (iv) the counterion. When the counterion is displaced, this creates an empty docking site at the metal center. The metal center seeks to fill this docking site with monomer or other ligands to regain its four-coordinate environment. It can partially fill this empty coordination site by forming a partial bond to an ortho ligand substituent capable of donating electron pairs. Ortho substituents that have electron pairs available for coordination to the metal include halogens, aromatic rings, and methoxy groups. Ortho substituents that do not have any electron pairs available for coordination to the metal include H and aliphatic groups (e.g., Me, Et, ^{i}Pr).

Determination of Chain Initiation and Propagation Rate Constants. Table 4 gives an overview of the experimental 1-hexene polymerization data. The experimental conditions, polymer molecular weight, polydispersity index (PDI) defined as M_w/M_n, k_p, and k_i/k_p are given. The PDI values are between 1 and 3, which is consistent with a single-site behavior. For polymerizations in toluene or bromobenzene solvent, the monomer versus time concentration profiles were fit to a simple kinetic model containing chain initiation, propagation, and catalyst deactivation steps to determine the rate constants:

$$\textbf{initiation:}\quad C + M \xrightarrow{k_i} CM \tag{5}$$

$$\textbf{propagation:}\quad CM_N + M \xrightarrow{k_p} CM_{N+1} \text{ for } N \geq 1 \tag{6}$$

$$\textbf{deactivation:}\quad CM_N + M \xrightarrow{k_d} DM_{N+1} \text{ or } CM_N \xrightarrow{k_d} DM_N \text{ for } N \geq 1 \tag{7}$$

The fitted kinetic profiles and rate constants for catalysts **1a**−**18a** were previously reported.[11] The same procedure was also used to determine rate constants for catalysts **19a**−**24a**, **30a**, and **31a** from the monomer concentration versus time data and is described in the Supporting Information. (Precatalysts **25**−**29** were not synthesized.) The catalyst deactivation step was ignored if catalyst deactivation was negligible. In cases where catalyst deactivation was appreciable, the deactivation step was made either first or zero order in monomer concentration according to what was needed to fit the monomer concentration versus

(42) The **m**−O−Ar angles, **m**−X Wiberg bond indexes, and **m**−X distances for the cations and ion pairs of all catalysts are presented in the Supporting Information.

Table 4. Experimental 1-Hexene Polymerization Data for [Cp′m(OAr)Me]$^+$[MeB(C$_6$F$_5$)$_3$]$^-$ [a]

precat. no.	m	Cp′	OAr substituent	$\theta_{Cp'} + \theta_{OAr}$ (deg)	S	T (°C)	[M]$_0$ (M)	[M]$_0$:[C]$_0$	k_p[b] (M^{-1} s^{-1})	k_i/k_p[c]	init.	M_n (kDa)	PDI
1	Ti	Cp	2,6-Me$_2$-4-Br	257	Tol	0	1	200	0.16−0.22	≥0.02	facile	3.2	*h*
2	Ti	Cp	2,6-Et$_2$	261	Tol	0	1	100	0.25−0.34	≥0.03	facile	5.2	1.4
3	Ti	Cp	2,6-^{i}Pr$_2$	265	Tol	0	1	200	0.42	≥0.02	facile	6.2	1.3
4	Ti	Cp*	none	251	Tol	0	1	200	0.42	≥0.02	facile	4.4	1.9
5	Ti	Cp*	4-F	251	Tol	0	1	200	0.27	≥0.02	facile	4.7	1.9
6	Ti	Cp*	4-Cl	252	Tol	0	1	200	0.24	≥0.02	facile	5.3	2.0
7	Ti	Cp*	4-Br	251	Tol	0	1	200	0.26	≥0.02	facile	5.2	2.2
8	Ti	Cp*	4-Ph	251	Tol	0	1	200	0.38	≥0.02	facile	4.7	1.9
9	Ti	Cp*	4-^{t}Bu	251	Tol	0	1	200	0.48	≥0.02	facile	5.1	*h*
10	Ti	Cp*	2,6-Me$_2$	282	Tol	0	1	200	0.51	0.0014	slow	28.6	1.1
11	Ti	Cp*	2,6-Et$_2$	286	Tol	0	1	200	0.56−0.78	0.0003	slow	44.8	1.2
12	Ti	Cp*	2,6-^{i}Pr$_2$	290	Tol	0	1	200	0.60−0.92	0.0001	slow	62.4	1.5
13	Ti	Cp*	2-cyclohexyl	280[d] 282[p]	Tol	0	1	200	0.74	≥0.02	facile	17.3	1.5
14	Ti	Cp*	2,6-Me$_2$-4-Br	282	Tol	0	1	200	0.28	0.0014	slow	27.9	1.6
15	Ti	Cp*	2-CH$_2$Ph	268[d] 267[p]	Tol	0	1	200	0.27	≥0.02	facile	14.3	1.4
16	Ti	Cp*	2,3,5,6-Ph$_4$	317	Tol	0	1	200	1.36	≥0.02	facile	9.5	*h*
17	Ti	Cp*	3-OMe	252[d] 251[p]	Tol	0	1	200	0.25	≥0.02	facile	3.1	1.7
18	Ti	Cp*	4-OMe	251	Tol	0	1	200	0.20	≥0.02	facile	5.4	1.9
19	Ti	Cp	2,3,5,6-Ph$_4$	297	Tol	0	1	100	2.2	≥0.03	facile	9.7	1.5
20	Ti	Cp*	2-Br	272[d] 272[p]	Tol	0	1	500	5.0−6.1	≥0.006	facile	32.4	1.4
21	Ti	Cp*	2-Ph	280[d] 282[p]	Tol	0	1	200	3.1	≥0.02	facile	14.7	1.3
22	Ti	Ind	2,3,5,6-Ph$_4$	305	Tol	25	1	100	≥3[e]	≥0.01	facile	7.8	1.4
23	Ti	Ind	2,6-^{i}Pr$_2$	274	Tol	0	1	100	2.4	≥0.03	facile	4.7	1.7
					Tol	−20	1	100	0.6	≥0.03	facile	4.2	1.6
24	Zr	Cp*	2,3,5,6-Ph$_4$	304	Tol	25	1	100	negl.				
					BrB	25	0.5	100[f]	0.045[f]	≥0.03	facile	11.8	1.1
					BrB	25	1	200[f]	0.045[f]	≥0.02	facile	17.6	1.1
					DCB	25	1	100[f]	0.73[f]	≥0.005	*g*	13.2	1.1
30	Ti	Cp*	2,6-(OMe)$_2$	290	Tol	0	1	200	0.05	≥0.02	facile	7.2	2.9
31	Ti	Cp*	2,6-^{i}Pr$_2$-4-Br	289	Tol	0	1	200	0.55	9×10^{-5}	slow	44.9	1.8

[a] Legend: d, aryloxide substituent distal to initiating group; p, aryloxide substituent proximal to initiating group. [b] k_p values for catalysts **1**−**18** were taken from ref 11. [c] k_i values for catalysts **10**−**12** and **14** were taken from the Supporting Information of ref 11. [d] Distal conformation of catalyst. [e] All monomer consumed within 2 min. [f] The M_n values with extremely narrow molecular weight distributions indicate 65−70% of the metal sites are active in these experiments, giving M:C = 140−150 (for nominal 100:1) and 280 (for nominal 200:1) and k_p = 0.063 (bromobenzene) and 1.1 (1,2-dichlorobenzene) on a per active site basis. [g] Undetermined because the kinetic profile shows an induction period but this induction period does not have the same form as slow initiation kinetics first order in monomer. [h] Experimental data not available.

time profile. Chain initiation was considered facile if there was no visible induction period at the beginning of the log monomer concentration versus time plot, and in this case only a lower bound can be placed on the value of k_i. If there was a visible induction period, chain initiation was considered slow and separate k_i and k_p values were determined via simultaneous optimization to fit the monomer concentration versus time profile and the M_n value.

For the moment, consider the case of a catalyst that does not deactivate and has chain initiation and propagation that are both first-order in monomer as given in eqs 5 and 6. The rate expression for monomer consumption is given by

$$\frac{d[M]}{dt} = -k_i[M][C] - k_p([C]_0 - [C])[M] \text{ where } \frac{d[C]}{dt} = -k_i[M][C] \quad (8)$$

which can be written in the dimensionless form

$$\frac{d\bar{M}}{d\tau} = \underbrace{-\bar{M}\bar{C}\zeta\left([C]_0/[M]_0\right)}_{\text{initiation}} - \underbrace{\bar{M}\left(1-\bar{C}\right)}_{\text{propagation}} \quad \text{where} \quad \frac{d\bar{C}}{d\tau} = -\zeta\bar{M}\bar{C} \quad (9)$$

where $\tau = k_p[C]_0 t$, $\zeta = (k_i/k_p)([M]_0/[C]_0)$, $\bar{M} = [M]/[M]_0$, and $\bar{C} = [C]/[C]_0$. The term in eq 9 containing the ratio $[C]_0/[M]_0$ accounts for monomer consumption due to chain initiation. Since the total amount of monomer consumed by chain initiation compared to chain propagation during the batch reaction is negligible whenever $[C]_0/[M]_0 \leq 0.01$, the numerical solution to eq 9 was found to be independent of $[C]_0/[M]_0$ whenever $[C]_0/[M]_0 \leq 0.01$. Equation 9 was solved numerically and is shown in Figure 7.

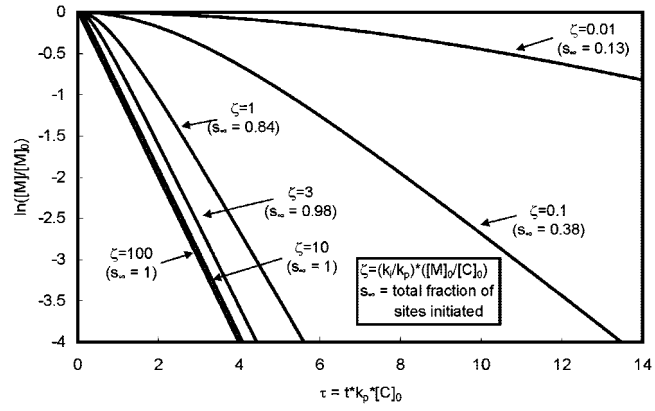

Figure 7. Dimensionless kinetic profiles for a batch polymerization reaction with first order in monomer chain initiation and propagation in the absence of catalyst deactivation.

The parameter ζ that defines the character of the kinetics depends upon both the k_i to k_p ratio and the initial concentration of monomer to catalyst, i.e. $[M]_0/[C]_0$. Examining Figure 7, one can see that when $\zeta > 3$ the induction period at the beginning of the reaction is negligible and chain initiation is facile. On

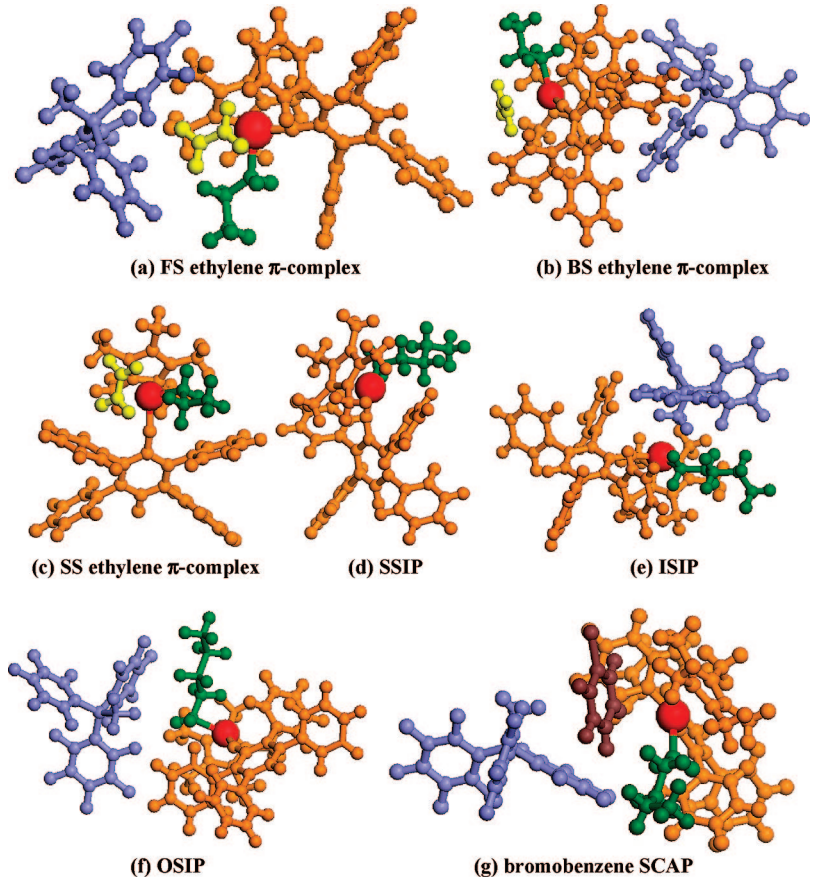

Figure 8. Different forms of π-complexes and ion pairs for catalyst **24a**: (red) metal; (green) growing chain; (lavender) counterion; (orange) ligands; (yellow) monomer; (brown) solvent.

Table 5. Effect of Solvent on [Cp*Zr(OC$_6$H-2,3,5,5,6-Ph$_4$)CH$_2$CH$_2$CH$_3$]$^+$[MeB(C$_6$F$_5$)$_3$]$^-$ Ethylene π-Complex and Product Formation Energies

		rel SCF energy (kcal/mol)			
	Zr−B (Å)	vacuum	toluene	bromobenzene	1,2-dichlorobenzene
		Reactants			
ISIP + ethylene	4.32	0	0	0	0
		π-Complexes			
FS π-complex	7.91	8.7	4.4	2.2	1.2
BS π-complex	9.09	14.4	6.9	3.6	2.0
SS π-complex	∼13	n.a.	11.2	4.6	2.0
		Products			
ISIP	4.32	−17.7	−17.5	−16.7	−16.5
β-agostic OSIP	7.55	−10.5	−17.1	−19.8	−21.1
SCAP	8.65 (Tol) 8.11 (BrB)	n.a.	−4.4	−4.9	n.a.
β-agostic SSIP	∼13	n.a.	−12.8	−19.4	−22.0

the other hand, when $\zeta < 3$ the induction period at the beginning of the batch reaction is appreciable and chain initiation is slow. In this case, some of the catalyst sites remain uninitiated even as the reaction proceeds to completion. For example, when $\zeta = 1$, 0.1, and 0.01 the fractions of sites initiated as t approaches infinity, s_∞, are 0.84, 0.38, and 0.13, respectively. When $\zeta < 0.1$, more than 62% of the sites remain uninitiated throughout the course of the batch reaction.

When a significant number of the sites remain uninitiated when the monomer is completely consumed and when chain transfer/termination steps are negligible, the final number of mers in a chain will exceed the initial monomer to catalyst ratio. For example, if only 10% of the catalyst sites are initiated throughout the course of a batch reaction having a 100:1 initial monomer to catalyst ratio, the average chain length produced will be 1000 mers, assuming the absence of chain transfer and termination. Thus, slow chain initiation can lead to longer polymer chains. For 100:1, 200:1, and 500:1 monomer to catalyst ratios, living polymerization of 1-hexene with facile initiation corresponds to 8.4, 16.8, and 42 kDa, respectively. Table 4 shows that in every case where chain initiation is slow the polymer M_n was more than 1.5 times these values. On the other hand, for every case with facile chain initiation, the polymer M_n was found to be either much less than or approximately equal to these values. The experimentally measured M_n values confirm the fact that only a few of the sites are active when chain initiation is slow. The cutoff for slow versus facile chain initiation does not occur at a k_i/k_p ratio of 1; rather, it occurs at the value $\zeta = 3$, which corresponds to a k_i/k_p ratio of $3[C]_0/[M]_0$. For a 200:1 monomer:catalyst ratio, the cutoff for facile versus slow initiation occurs at $k_i/k_p = 0.015$.

The catalysts can be divided into the following basic categories, according to whether chain initiation and chain transfer/termination are facile or slow.

(1) Chain initiation is facile and chain transfer/termination is facile. Facile chain transfer/termination causes the M_n value to be substantially below that expected for a living polymerization. This category included catalysts **1a**−**9a**, **17a**, **18a**, and **23a**, for which M_n values were 6 kDa or less. These are the most sterically open catalysts, with $\theta_{Cp'} + \theta_{OAr}$ ranging from 251 to 274°. This category contained (a) all of the Cp* catalysts with two trivial ortho substituents (i.e., 2,6-H$_2$) and (b) all of the Cp and Ind catalysts except for those containing the largest ArO ligand (i.e., 2,3,5,6-Ph$_4$).

(2) Chain initiation is facile, chain transfer/termination is slow, and all of the metal sites are active. This category contained

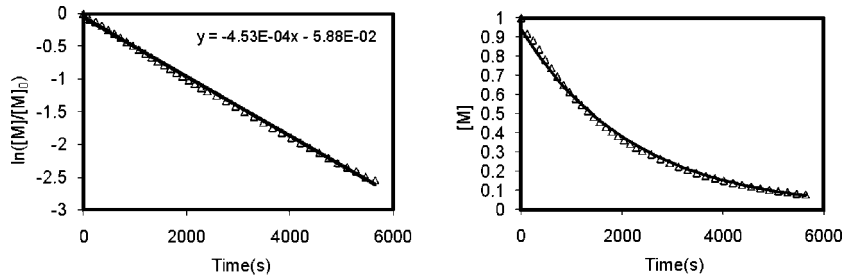

(a) 100:1 monomer to catalyst ratio in bromobenzene

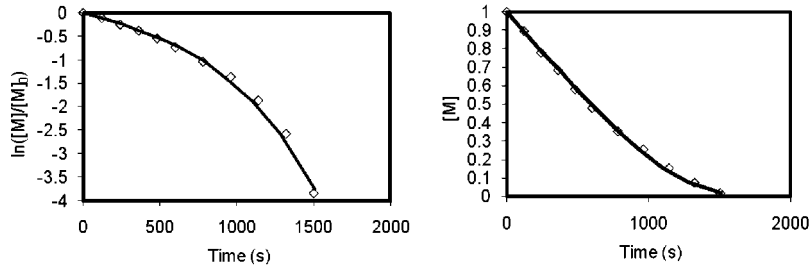

(b) 100:1 monomer to catalyst ratio in 1,2-dichlorobenzene

Figure 9. Effects of solvent on the reaction rate and order: monomer concentration versus time profiles for 1-hexene polymerization catalyzed by $[Cp^*Zr(OC_6H\text{-}2,3,5,6\text{-}Ph_4)Me]^+[MeB(C_6F_5)_3]^-$ in bromobenzene and 1,2-dichlorobenzene at room temperature. Solid lines are the kinetic model fits described in the text.

Scheme 2. Chain Initiation and Propagation Reactions

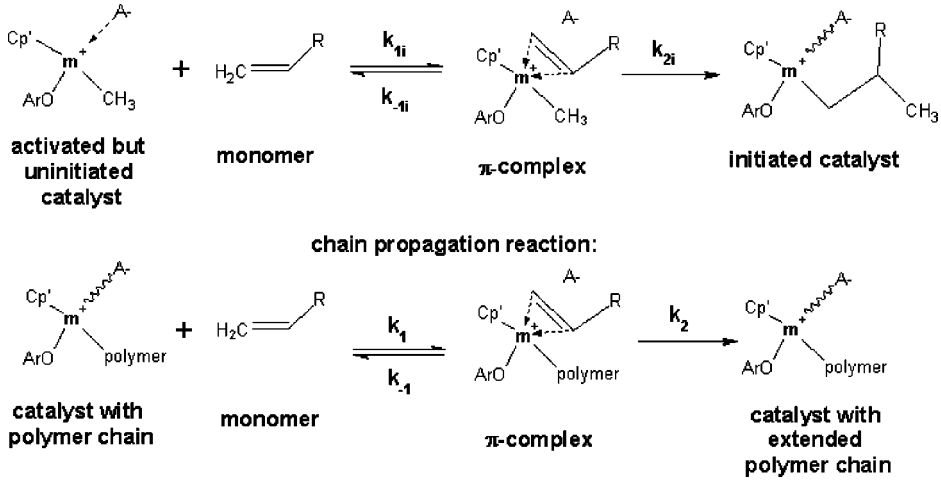

catalysts for which the M_n value was between 43 and 103% of that which would be expected from a living polymerization. Category 2 included catalysts **13a**, **15a**, **16a**, **19a**−**22a**, and **30a**, which have $\theta_{Cp'} + \theta_{OAr}$ in the range of 267−317°. This category contained the Ti-based catalysts with (a) Cp* plus one nontrivial ortho aryloxide substituent, (b) Cp, Ind, or Cp* with the 2,3,5,6-Ph_4 substituted ligand, and (c) Cp* catalysts for which one or both ortho ayloxide substituents can opportunistically coordinate to the metal center upon ion pair separation.

(3) Chain initiation is slow and chain transfer/termination is slow. This category included the catalysts **10a**−**12a**, **14a**, and **31a**. For these catalysts, the M_n values ranged from 166 to 371% of the value expected for a living polymerization. The total ligand cone angles $\theta_{Cp'} + \theta_{OAr}$ ranged from 282 to 290°. This category contained all Cp* catalysts with two nontrivial ortho substituents where neither of these substituents opportunistically coordinates to the metal center.

(4) Chain initiation is facile, chain transfer/termination is slow, but not all of the metal sites are active. This category contained the Zr-based catalyst **24a**. For this catalyst, the M_n value was approximately 140% of that expected for living polymerization. Combined with the narrow molecular weight distribution (PDI = 1.1), this suggests only 65−70% of the metal sites are active for polymerization. The percentages of active sites were approximately the same in bromobenzene and 1,2-dichlorobenzene solvents. The reason only some of the metal sites are active is not fully understood at this time.

Different Types of Ion Pair and π-Complex States. As mentioned in the Introduction, ion pairs can exist as either ISIP, OSIP, SCAP, or SSIP. There is competition between counterion, monomer, solvent, ligand, and initiating group or growing polymer chain for the docking site at the metal center. The counterion occupies the docking site in an ISIP, while the solvent occupies the docking site in an SCAP. In the outer-sphere and solvent-separated states, monomer, ligand, solvent, initiating group, or growing polymer chain occupies the docking site. The ligand, initiating group, or growing polymer chain can potentially occupy the docking site only if it has a chemical structure

that allows it to opportunistically, fluxionally, or agostically bond to the metal center upon partial ion pair separation.

The geometries (Figure 8) and relative energies (Table 5) of different ion pair and π-complex states were computed for catalyst **24a**. For this catalyst, the OSIP and SSIP contained opportunistic bonding from the aryloxide ligand and β-agostic bonding from the growing polymer chain to the metal center. The Zr−B distance increased from 4.32 Å in the ISIP to 7.55 Å in the OSIP and 8.11 Å in the bromobenzene SCAP. The charge separation distance in the SSIP state was estimated as approximately 13 Å by adding twice the solvent radius (2.82 Å) to the Zr−B distance in the OSIP state and rounding to the nearest angstrom.

Geometry optimization of the SCAP states was started with an initial guess of η^6 coordination by a solvent molecule to the metal center. In the case of 1,2-dichlorobenzene the solvent molecule was displaced to the outer coordination sphere, indicating that an SCAP state is not formed. In the case of toluene and bromobenzene, the converged geometry contained a solvent molecule in the inner coordination sphere with η^1 coordination, which suggests η^6 coordination of the solvent to the metal is not favorable for **24a**. In toluene and bromobenzene, the SCAP states were 8.4−14.9 kcal/mol higher in energy than the ISIP, OSIP, and SSIP. Because the SCAP is the least favored of the four different ion pair forms, it follows that solvent is a poor competitor for the docking site.

The relative SCF energies of different ion pair forms were found to be a strong function of solvent. Under vacuum, the ISIP was much lower in energy than any of the other ion pairs. In toluene, the ISIP and OSIP were approximately tied for the lowest energy, while the SCAP and SSIP were substantially higher in energy. In bromobenzene, the computed relative energies of the ISIP, OSIP, and SSIP were within 3 kcal/mol of each other, while the SCAP was much higher in energy. Since the absolute accuracy of the DFT method is ca. ±5 kcal/mol, it is not clear which of these three ion pair forms is actually the most stable in bromobenzene. In 1,2-dichlorobenzene, the SSIP and OSIP were approximately tied for the lowest energy while the ISIP was approximately 5 kcal/mol higher in energy. These results clearly show the trend that ISIP and/or OSIP are preferred in lower dielectric constant solvents while SSIP and/or OSIP are preferred in higher dielectric constant solvents.

The counterion can occupy different positions in the π-complexes: (a) the front-side (FS) π-complex has the monomer and counterion on the same side of the cation and (b) the back-side (BS) π-complex has the monomer and counterion on opposite sides of the cation. In the FS and BS π-complexes, the counterion is in the outer coordination sphere of the metal, while the counterion is fully solvated in the solvent-separated (SS) π-complex. In each solvent, the FS π-complex was lower in energy than the SS and BS π-complexes. This is explained by the smaller ion pair separation distance in the FS (Zr−B = 7.91 Å, Table 5) versus the BS (9.09 Å) and SS (∼13 Å) π-complexes. In general, the energy required to form a π-complex is the sum of two competing effects: (1) the energy cost associated with partial separation of the ion pair and (2) the energy gain associated with the monomer forming a bond to the metal center. As K_S increases, the energy cost of partial ion pair separation decreases, causing the π-complex formation energy to also decrease. For example, the computed energy to form the FS π-complex decreased from 8.7 kcal/mol under vacuum to only 1.2 kcal/mol in 1,2-dichlorobenzene, while that for the BS π-complex decreased from 14.1 kcal/mol under vacuum to 2.0 kcal/mol in 1,2-dichlorobenzene.

Effects of Solvent on Reaction Order. Figure 9 shows monomer concentration versus time profiles for catalyst **24a** in bromobenzene and 1,2-dichlorobenzene solvents at room temperature. Kinetic data are not available for toluene, since the reaction rate was negligible. For each solvent, normal and semilog plots are shown. First order in monomer chain propagation with facile chain initiation and negligible catalyst deactivation leads to a straight line on the semilog plot, while a zero order in monomer propagation with facile initiation and negligible deactivation leads to a linear monomer concentration versus time plot. In bromobenzene, the kinetic profile is linear on a semilog plot; thus, the propagation is apparently first order in monomer and initiation is facile. In 1,2-dichlorobenzene, the chain propagation starts out as zero order in monomer, since the linear monomer concentration versus time plot is observed, but the kinetics then transitions to first order as monomer is consumed.

A candidate mechanism for transition from zero- to first-order monomer consumption during a batch reaction is developed here. Consider a simple model of chain propagation in which the monomer reversibly coordinates to an ion pair to form a π-complex followed by insertion of the coordinated monomer to elongate the polymer chain (Scheme 2); specifically

$$\mathrm{IP} + \mathrm{M} \underset{k_{-1}}{\overset{k_1}{\rightleftharpoons}} \Pi \xrightarrow{k_2} \mathrm{IP} \tag{10}$$

The coordination and insertion steps are repeated many times to produce the polymer chain. A similar kinetic mechanism for a steady-state reactor has been previously considered.[43] Now the batch reactor kinetics are developed. The terms IP and Π in these equations refer to the kinetically most important ion pair and π-complex states. Which particular ion pair (ISIP, OSIP, SCAP, or SSIP) and π-complex (FS, BS, or SS) is the kinetically most important depends upon the catalyst structure, solvent, and other reaction conditions. The concentration of live catalyst sites is given by

$$[C_{\mathrm{live}}] = [\mathrm{IP}] + [\Pi] \tag{11}$$

Since the catalyst undergoes many turnovers during the course of polymerization, we can utilize the pseudo-steady-state approximation:

$$0 \approx \frac{\mathrm{d}[\Pi]}{\mathrm{d}t} = k_1[\mathrm{IP}][\mathrm{M}] - (k_{-1} + k_2)[\Pi] \tag{12}$$

which combined with the site balance gives

$$[\Pi] = \frac{k_1[\mathrm{M}][\mathrm{C_{live}}]}{k_1[\mathrm{M}] + k_{-1} + k_2} \text{ and } [\mathrm{IP}] = \frac{(k_{-1} + k_2)[\mathrm{C_{live}}]}{k_1[\mathrm{M}] + k_{-1} + k_2} \tag{13}$$

The propagation rate for a batch reaction is thus given by

$$-\frac{\mathrm{d}[M]}{\mathrm{d}t} = k_2[\Pi] = \frac{k_1k_2[\mathrm{C_{live}}][\mathrm{M}]}{k_1[\mathrm{M}] + k_{-1} + k_2} \tag{14}$$

Equation 14 is integrated to give

$$\int_0^t \mathrm{d}t = t = -\int_{[\mathrm{M}]}^{[\mathrm{M}]_0} \frac{k_1[\mathrm{M}] + k_{-1} + k_2}{k_1k_2[\mathrm{C_{live}}][\mathrm{M}]}\,\mathrm{d}[\mathrm{M}] = \frac{1}{[\mathrm{C_{live}}]}\left(\frac{1}{k_2}([\mathrm{M}]_0 - [\mathrm{M}]) - \frac{1}{k_p}\ln\left(\frac{[\mathrm{M}]}{[\mathrm{M}]_0}\right)\right) \tag{15}$$

where the effective propagation rate constant is given by

$$k_p = \frac{k_1 k_2}{k_{-1} + k_2} \tag{16}$$

Equation 15 provides a good fit to the experimental data, as shown in Figure 9, where the fitted parameters for **24a** in 1,2-dichlorobenzene are $k_p = 0.73\ M^{-1}\ s^{-1}$ and $k_2 = 0.1\ s^{-1}$, and normalizing for the percentage of active sites at 65% gives $k_p = 1.1\ M^{-1}\ s^{-1}$ and $k_2 = 0.15\ s^{-1}$.

On examination of the denominator in eq 14, the value of the dimensionless group

$$G = \frac{k_1[M]}{k_{-1} + k_2} = \frac{[\Pi]}{[IP]} \tag{17}$$

is related to whether chain propagation is zero or first order in monomer. Chain propagation is zero order when $G \gg 1$ and first-order when $G \ll 1$. If the π-complex formation energy is substantially positive, one predicts $[\Pi] \ll [IP]$ and thus first-order in monomer propagation. If the π-complex formation energy is substantially negative, one predicts $[\Pi] \gg [IP]$ and thus zero-order in monomer propagation. If the π-complex formation energy is close to 0, one predicts $[\Pi] \approx [IP]$ and chain propagation may transition between zero and first order. The decrease in π-complex formation energy as K_S increases leads to increasing G, which can cause the reaction to transition from first to zero order in monomer as K_S increases. This provides a possible explanation for why the chain propagation reaction for catalyst **24a** was first order in monomer for bromobenzene solvent but combined zero and first order for 1,2-dichlorobenzene solvent.

Structure−Activity Correlation for Chain Propagation

Previously we reported a structure−activity correlation for 1-hexene chain propagation rate constants for a series of Ti mixed Cp′/ArO catalysts activated with $B(C_6F_5)_3$ in toluene solvent.[11] This structure−activity correlation was based on the observation that monomer access to the metal center is the key factor controlling the reactivity of these catalysts. Monomer access to the metal is in turn controlled by steric congestion and the difficulty of partial ion pair separation. Ligand cone angles were used to quantify the amount of steric congestion at the metal, while E_{IPS} was used to quantify the difficulty of ion pair separation. The structure−activity correlation took the form of an Arrhenius-like equation:

$$k_p = k_0 e^{-E_a/RT} = \gamma a_0 \exp\left[\frac{-1}{RT}(E_0 + \alpha E_{IPS})\right] \tag{18}$$

The activation energy was linearly correlated to E_{IPS} in solution by

$$E_a = E_0 + \alpha E_{IPS} \tag{19}$$

The pre-exponential factor was linearly correlated to the free solid angle $4\pi\gamma$ for monomer approach to the metal center

$$k_0 = \gamma a_0 \tag{20}$$

where the free solid angle for monomer approach was computed by subtracting the solid angles occupied by each of the ligands:

$$\gamma = \text{the larger of } (1 - \sin^2(\theta_{Cp'}/4) - \sin^2(\theta_{OAr}/4) - f) \text{ and } 0 \tag{21}$$

The parameter f accounts for space blocked by the growing polymer chain and partially displaced counterion and was fitted from the data.

The activation energy E_a and pre-exponential factor k_0 are experimentally measurable quantities; thus, their values should be independent of any of the computational methods employed to generate the catalyst descriptors. Since the slope of the linear correlation between B3LYP and OLYP E_{IPS} values is approximately 1, irrespective of basis set, it follows from eq 19 the adjustable parameter α is the same for both functionals and independent of basis set. From the average E_{IPS} differences, it follows from eq 19 that the value of the adjustable parameter E_0 is approximately $\alpha \times 10$ kcal/mol = 3 kcal/mol higher when using OLYP than when using B3LYP E_{IPS} values. For each catalyst, the computed ligand cone angles were virtually unaffected by the choice of exchange-correlation functional and basis set. For example, catalyst **1a** gave $\theta_{Cp'} = 128°$ (OLYP/6-311++G**), 128° (OLYP/LANL2DZ), 129° (B3LYP/6-311++G**), 128° (B3LYP/LANL2DZ) and $\theta_{OAr} = 129°$ (OLYP/6-311++G**), 129° (OLYP/LANL2DZ), 130° (B3LYP/6-311++G**), 130° (B3LYP/LANL2DZ). Because the computed ligand cone angles are independent of basis set and functional choice, it follows from eqs 20 and 21 that the adjustable parameters a_0 and f are likewise unaffected by a change in basis set or exchange-correlation functional.

The structure−activity correlation for k_p depends upon (i) the quantitative descriptors E_{IPS}, $\theta_{Cp'}$, and θ_{OAr} that are computed theoretically and (ii) adjustable parameters α, f, E_0, and a_0 that are fit using a training set of experimental data. Similar catalysts are grouped into families such that all catalysts in a single family have the same values of the adjustable parameters. The parameters α and E_0 could potentially be computed by purely theoretical means by regressing a series of DFT-computed E_a values to E_{IPS} values to determine the slope α and intercept E_0 for a given family. The steric factor f accounting for space blocked by the growing chain and partially displaced counterion should be constant for a given monomer and counterion, while a_0 just scales the reaction rate for the whole catalyst family. Thus, the parameters are actually a very small set and all have a clear physical meaning. Since all of the catalysts in a single family have the same values of the adjustable parameters and the quantitative descriptors can be computed theoretically, it is possible to predict the k_p value ahead of time for a new catalyst in an established family.

Since the reactions were all performed at 0 °C, a_0 and E_0 were absorbed into a parameter $A = a_0 \exp(-E_0/RT)$ that was optimized for each catalyst family. We propose that mixed Cp′/ArO catalyst families are determined according to the following factors: (a) the metal center, i.e. Zr or Ti, (b) the structure of the Cp′ ligand, i.e. Cp, Ind, Cp*, etc., (c) the initiating group, i.e. methyl, benzyl, etc., (d) the counterion, i.e. $[MeB(C_6F_5)_3]^-$, $[B(C_6F_5)_4]^-$, etc., (e) whether or not the aryloxide ligand contains non-H substituents in both ortho positions, (f) whether or not the aryloxide ligand contains at least one ortho substituent that can opportunistically bond to the metal, and (g) whether or not the aryloxide ligand contains substituents that can potentially lead to undesirable coordination to the activator or a second catalyst center, e.g. methoxy substituents.

Catalysts in the same family have similar features in categories a−g above. The division of catalysts into different families is necessary in part because basic structural changes cause the catalyst's kinetic behavior to change. For example, Cp* catalysts with two ortho alkyl substituents on the aryloxide ring (e.g., **10a**−**12a**, **14a**, **31a**) had slow chain initiation and slow chain transfer. Catalysts with opportunistically bonding ligands (e.g., **16a**, **19a**−**22a**, **24a**, **30a**) had facile chain initiation irrespective of the amount of steric congestion. Cp* catalysts

with zero or one ortho substituent on the aryloxide ring (**4a**−**9a**, **13a**, **15a**, **17a**, **18a**, **20a**, **21a**) had facile chain initiation but slow chain transfer. Cp catalysts with two ortho Me, Et, or ^{i}Pr substituents on the aryloxide ring (**1a**−**3a**) had facile chain initiation and facile chain transfer.

The experimental data for catalysts **1a**−**18a** were previously fit to the above equations to yield optimized values $\alpha = 0.300$ and $f = 0.187$.[11] The new catalyst **31a** provides a test of this correlation, because it falls into a family for which the parameter A is known. Using the parameter $A = 2.65 \times 10^7$ M^{-1} s^{-1} for this family and the computed E_{IPS} and ligand cone angles, the predicted propagation rate constant is 0.64 M^{-1} s^{-1} for 1-hexene polymerization in toluene at 0 °C, which is in good agreement with the experimental value of $k_p = 0.55$ M^{-1} s^{-1}.

Effect of Solvent. A change in solvent affects E_{IPS} but not the ligand cone angles. If the parameters α, f, E_0, and a_0 are presumed to be similar in different solvents, this corresponds to the following ratio of rate constants:

$$\frac{k_p[\text{solvent}_2]}{k_p[\text{solvent}_1]} \cong \exp\left(\frac{\Delta E_a}{RT}\right) \qquad (22)$$

where

$$\Delta E_a \cong \alpha(E_{IPS}[\text{solvent}_1] - E_{IPS}[\text{solvent}_2]) \qquad (23)$$

Equation 22 can be used to predict the dependence of k_p on solvent if the reaction mechanisms are the same in both solvents. This requires that the metal docking site be occupied by the same electron donor system (i.e., counterion, solvent, ligand, or growing chain) in the kinetically dominant form of IP in both solvents; however, the overall reaction order need not be the same in both solvents, since the same reaction mechanism can give rise to different overall reaction orders.

For catalyst **24a** in bromobenzene and 1,2-dichlorobenzene, the docking site is occupied by an H atom from the growing polymer via β-agostic bonding. In both of these solvents, the monomer must displace this H atom from the docking site in order to form the π-complex and the counterion acts only as a spectator. Since the reaction mechanisms are similar, the ratio of k_p values in bromobenzene and 1,2-dichlorobenzene can be estimated using eq 23. Using $\alpha = 0.3$, the predicted lowering of activation energy for 1-hexene polymerization by catalyst **24a** upon changing from bromobenzene to 1,2-dichlorobenzene solvent is 1.52 kcal/mol. At 25 °C this corresponds to a predicted increase in k_p by a factor of 13. As shown in Table 4, the experimentally measured ratio was 16, which is in reasonable agreement.

Effect of Counterion. As a result of weaker counterion binding of $[B(C_6F_5)_4]^-$ versus $[MeB(C_6F_5)_3]^-$, the rate of polymerization is expected to increase significantly upon changing $[MeB(C_6F_5)_3]^-$ to $[B(C_6F_5)_4]^-$. This agrees with the experimental results given in Table 2, where the 1-hexene polymerization activity increased by a factor of 20−50 for catalysts **10**−**12** upon changing $[MeB(C_6F_5)_3]^-$ to $[B(C_6F_5)_4]^-$.

A rigorous prediction of the dependence of polymerization rate on counterion should take into consideration changes in the counterion size and other factors. These factors can be included implicitly in the above structure−activity correlation by using different catalyst families for $[MeB(C_6F_5)_3]^-$- and $[B(C_6F_5)_4]^-$-based catalysts. However, a rough prediction of the rate increase upon switching from $[MeB(C_6F_5)_3]^-$ to $[B(C_6F_5)_4]^-$ can be made by assuming the parameters α, f, E_0, and a_0 are similar for the two counterions. Using these simplifications, the increase in activity upon changing from $[MeB(C_6F_5)_3]^-$ to $[B(C_6F_5)_4]^-$ is approximated by $\exp(\alpha(E_{IPS}[MeB(C_6F_5)_3] - E_{IPS}[B(C_6F_5)_4])/RT)$ and is shown in Table 2. This initial prediction underestimates the experimental ratios by a factor of ca. 2.2, and this suggests the family parameter $A = a_0 \exp(-E_0/RT)$ for the $[Cp^*Ti(OC_6H_3\text{-}2,6\text{-}R_2)Me]^+[B(C_6F_5)_4]^-$ family is about 2.2 times that for the $[Cp^*Ti(OC_6H_3\text{-}2,6\text{-}R_2)Me]^+[MeB(C_6F_5)_3]^-$ family. This adjustment is taken into consideration to give the refined predictions displayed in the last column of Table 2, and these values are in good agreement with experiment.

Effects of Opportunistic Ligand Coordination. Computational investigation into the experimentally observed high reactivity of **16a** led to the discovery that an opportunistically coordinating group in the ortho position of the aryloxide ring can greatly enhance the catalyst reactivity by lowering E_{IPS}. Additional experiments and computations showed that, to minimize steric congestion, this group should only be placed in one of the ortho positions. Placement of the group in both ortho positions (e.g., 2,3,5,6-Ph$_4$ **16a**) can lead to lower reactivity compared to placement of the group in one ortho position (e.g., 2-Ph **21a**) due to the very high steric congestion associated with Cp* 2,6-substituted aryloxide complexes. Synthesis of catalyst **20a** was motivated by computations showing that an ortho Br substituent exhibits stronger opportunistic coordination and lower E_{IPS} than an ortho phenyl substituent. The k_p value of **20a** was subsequently found to be the highest of any of the catalysts we investigated. This is a clear demonstration that the proposed structure−activity correlation can be used to design a more reactive catalyst.

The system $Cp^*Ti(OC_6H_4\text{-}2\text{-}X)Me_2/B(C_6F_5)_3$ for X = F, Cl, Br, I, Ph forms a family of similar catalysts that have lower E_{IPS} and presumably higher reactivity than the corresponding $Cp^*Ti(OC_6H_4\text{-}4\text{-}X)Me_2/B(C_6F_5)_3$ catalysts. For example, catalyst **20a** (2-Br) has E_{IPS} 7.89 kcal/mol lower[44] and a k_p value about 21 times higher than for **7a** (4-Br). Catalyst **21a** (2-Ph) has E_{IPS} 5.51 kcal/mol lower and a k_p value about 8.2 times higher than for **8a** (4-Ph). At the present time, there is not enough experimental data to accurately determine the parameters α and A for this family; however, anticipated reactivity trends can still be predicted for different catalysts in this family. Catalyst **28a** (2-I), which has not been synthesized, is anticipated to have even higher reactivity than catalyst **20a** (2-Br), due to its lower E_{IPS} and similar steric congestion. The remaining catalysts in this series, **26a** (2-F) and **27a** (2-Cl), have higher E_{IPS} values and are anticipated to have lower k_p values than **20a** (2-Br).

Effect of Metal. When the structure of the Cp′/ArO catalyst is held constant except for a change in metal from Ti to Zr, there is a large increase in E_{IPS} but only a slight decrease in steric congestion. For example, the Ti-based catalyst **16a** has an E_{IPS} value in toluene that is 6.1 kcal/mol lower than for the Zr analogue (catalyst **24a**), but $\theta_{Cp'} + \theta_{OAr}$ is only 13° higher for **16a** than for **24a**. Due to the tighter counterion binding, monomer coordination is more difficult for **24a** compared to **16a**. Catalyst **16a** is reactive in toluene, while **24a** is not. To compensate for the tighter counterion binding in the Zr-based system, it was necessary to use the Zr-based catalyst in a more polar solvent such as bromobenzene or 1,2-dichlorobenzene. In bromobenzene, catalyst **16a** consumed all monomer within

(43) Marques, M. M.; Dias, A. R.; Costa, C.; Lemos, F.; Ribeiro, F. R. *Polym. Int.* **1997**, *43*, 77–85.

(44) For this catalyst family, the average of E_{IPS} values for the proximal and distal conformations have been used, since these conformations have similar total energies and E_{IPS} values.

2 min, while catalyst **24a** had a slow but measurable polymerization rate. In addition, the rate constant k_2 for insertion proper is lower for the Zr-based catalyst **24a** than for the Ti-based analogue. Specifically, for catalyst **24a** in 1,2-dichlorobenzene $k_2 = 0.1-0.15\ s^{-1}$, and for catalyst **16a** in toluene the initial turnover rate was $0.9\ s^{-1}$, giving $k_2 \geq 0.9\ s^{-1}$. The value of k_2 should be relatively insensitive to a change in the dielectric constant K_S of solvent, since the ion pair separation distance is nearly constant during insertion proper.

The slower rate of **24a** compared to that of **16a** is due to both higher E_{IPS} leading to slower monomer coordination and lower k_2 leading to slower insertion proper. These two factors combine to make **24a** orders of magnitude less reactive than its Ti-based analogue **16a**. Because the intrinsic rate of monomer insertion, k_2, is different for these two metals, Ti and Zr catalysts should not be classified into the same family in the structure−activity correlation described above.

Discussion

A systematic study of the relationship between the rate of chain propagation and the catalyst structure as computed via DFT has been reported for a series of aryloxide-ligated Ti and Zr single-site catalysts for the polymerization of 1-hexene, where the effects of solvent, metal, counterion, and ligand structure were investigated. Significant findings include the following.

(1) The data support a previously developed structure−activity model.[11] The rate of propagation is determined by the difficulty of the monomer to gain access to the metal center and form a π-complex, and the rate of propagation is a function of the ion pair separation energy and the steric congestion at the catalytic site, as described by the cone angles of the ligands and growing polymer chain.

(2) The effect of the type of solvent on the ion pair separation energy, and hence the rate of propagation, is determined by electrostatics, where E_{IPS} is a linear function of K_S^{-1} (see eq 3) and K_S is the solvent's dielectric constant.

(3) For catalyst **24a** the monomer consumption was first order in bromobenzene, but when the solvent was changed to 1,2-dichlorobenzene with a higher dielectric constant, the reaction was initially zero order but changed to first order as the reaction proceeded. This change in reaction order with solvent and during the course of reaction can be quantitatively explained, assuming formation of the π-complex is a reversible reaction and the insertion of the monomer to increase the chain length is an irreversible reaction. The overall reaction (i) is zero order in monomer if the π-complex formation energy is substantially negative, (ii) is first order if the π-complex formation energy is substantially positive, and (iii) exhibits a transition from zero order to first order if the π-complex formation energy is approximately 0.

(4) It was observed that ligands with ortho substituents capable of donating electrons that can opportunistically bond with the metal center, as determined by the Wiberg bond index, have a significantly lower E_{IPS} and consequently a much faster rate of propagation.

(5) Consistent with simple electrostatic arguments, DFT simulations indicate that in lower dielectric constant solvents the catalyst/counterion system exists as either an inner-sphere ion pair (ISIP) or an outer-sphere ion pair (OSIP), while in high dielectric constant solvents the system prefers to be an OSIP or solvent-separated ion pair (SSIP).

(6) DFT simulations indicate that Zr catalysts more tightly bind the counterion (i.e., the E_{IPS} is greater) than Ti catalysts with the same ligands and consequently the rate of propagation for Ti catalysts is greater than for the analogous Zr catalysts.

These findings provide additional evidence supporting the proposed quantitative structure−activity model for chain propagation, where the solvent affects the interaction between the metal center and counterion via dielectric shielding. We believe that this is the most extensive development of a quantitative structure−activity model for single-site polymerization catalysts to date and shows the value of quantitative modeling for these systems.

Other groups have also pursued the development of structure−activity models, which are consistent with the findings above. Chen and Marks report an inverse relationship between polymerization activity for five constrained-geometry catalysts and the free energy of activation, $\Delta G^{\ddagger}_{reorg}$, required for the counterion to separate from the metal center and redock following a chain swing.[6] They used two different metals (Ti, Zr) and three different counterions to generate the five catalysts, and all five catalysts had the same ligands. Because counterion binding strength is a major contribution to $\Delta G^{\ddagger}_{reorg}$, there is a strong relationship between the $\Delta G^{\ddagger}_{reorg}$ and E_{IPS} descriptors. A major difference is that $\Delta G^{\ddagger}_{reorg}$ is an experiment quantity; in contrast, E_{IPS} can be computed via DFT for a catalyst not yet synthesized. Counterion Lewis acidity strength, counterion size (i.e., van der Waals volume), ion pair formation energy from the precatalyst, and NMR shifts of the methyl initiating group are other quantitative descriptors that have been proposed to correlate the effects of counterion structure on the reactivity of single-site olefin polymerization catalysts.[4,6] These descriptors are limited because they require aspects of the catalyst structure to be held constant. Specifically, the first two descriptors do not consider the nature of the cation and thus cannot explain any changes in reactivity observed when the cation structure is changed. Ion pair formation energies and NMR shifts depend upon a variety of factors, including the metal and initiating group, in addition to counterion binding strength. In summary, E_{IPS} is a more appropriate quantitative descriptor of counterion binding strength, because (i) it is directly related to the energy required for the separation of the counterion required for the monomer to form the π-complex and (ii) it naturally accounts for variations in ligands, counterion, metal, and solvent.

Conclusion 5 above concerning the effect of the solvent's dielectric constant on the formation of different kinds of ion pairs is consistent with the experiments by Eisch et al. using multinuclear NMR.[14] Their experiments indicate that more polar solvents and higher dilution favor formation of an SSIP over an ISIP. They observed that small arene solvents favored formation of the SCAP, where σ or η^1 binding is postulated. Alternatively, larger arene solvents cannot form the SCAP due to steric limitations. These results are in general agreement with our computations showing that high-polarity solvents favor the SSIP over the ISIP and that smaller arenes may lead to the formation of η^1-bound SCAP. The relative reactivities of these ion pairs were found to be SSIP > ISIP > SCAP.[14]

There is no clear consensus in the literature regarding the effects of solvent polarity (K_S) on catalyst reactivity. In some cases, an increase in K_S leads to orders of magnitude increase in rate; in other cases, an increase in K_S leads to only a modest increase in rate; in yet other cases, an increase in K_S has almost no effect on the polymerization rate.[7,14,45] These results imply a threshold beyond which increasing K_S does not further enhance the catalyst reactivity, and this threshold is dependent upon the

(45) Klamo, S. B. Ph.D. Thesis; Chemistry Department, California Institute of Technology, 2005.

catalyst system under investigation. One potential explanation for this behavior is that increased K_S is expected to enhance the reaction rate only if an ISIP is the global ground state, since formation of monomer coordination and insertion proper transition states from ISIP requires partial ion pair separation; however, for solvents where an OSIP or SSIP is the global ground state, any further increase in K_S may have little effect on reactivity, since formation of monomer coordination and insertion proper transition states requires little (if any) further ion pair separation. Additional experiments are needed to validate this hypothesis

In addition to changing counterion and solvent polarity, we have shown that opportunistic ligand coordination can decrease E_{IPS} and thereby increase catalyst reactivity. Although flexible ligand bonding has been described in the literature for several group 4 single-site olefin polymerization catalysts,[6,46] to the best of our knowledge the specific use of flexible ligand bonding to decrease E_{IPS} has not been reported previously. In our picture, opportunistic ligand coordination involves a group attached to the ligand backbone that does not coordinate to the metal center in the ISIP, but the group partially coordinates to the metal center as the counterion leaves, thereby reducing E_{IPS}. The opportunistically coordinating group must be capable of exhibiting partial coordination to the metal center when the counterion is only partially displaced; otherwise, the opportunistic coordination does not facilitate the early stage of ion pair separation crucial for monomer approach to the metal center. The early stage of ion pair separation is crucial, because computations show only partial ion pair separation occurs in the monomer coordination transition states. Moreover, the opportunistically coordinating group should be located off to the side of the catalytic site in order to allow room for the approaching monomer to enter. We believe opportunistic ligand coordination is a potential strategy for decreasing the E_{IPS} of various of single-site olefin polymerization catalysts containing a counterion that must be displaced from the metal to allow formation of an olefinic π-complex. This provides a potential strategy for increasing the reactivity of a wide range of different single-site olefin polymerization catalysts.

Quantitative structure−activity relationships (QSARs) can potentially be used both to explain reactivity trends of existing catalysts and to intelligently design new catalysts. A key drawback of most existing QSARs for single-site olefin polymerization catalysis is that they correlate catalyst descriptors to activity rather than to rate constants.[47,48] For many olefin polymerization systems, catalyst initiation may not be facile, catalyst deactivation may be appreciable, and the percentage of active sites may be less than 100%; thus, the k_p value per active site can be significantly different from that indicated by simple activity measurements. Consequently, QSARs based on activity are of limited value, because they can only predict catalyst performance for a fixed set of reaction conditions. In contrast, a detailed microkinetic model can describe the effect of catalyst, monomer, cocatalyst, and/or activator concentration on the catalyst performance, where the various rate constants are subsequently correlated with the molecular structure of the various species. The development of a QSAR for the chain propagation rate constant discussed in this article is a significant improvement over the more traditional use of QSAR to model activity. To the best of our knowledge, there is only one other QSAR study for homogeneous group 4 single-site olefin polymerization catalysts that correlates quantitative descriptors to the chain propagation rate constant, k_p. Stovneng et al. developed a QSAR for ethylene polymerization for 9 unbridged zirconocenes activated with MAO.[49] Principal-component analysis followed by partial least-squares regression was used to correlate k_p and activity for 9 catalysts to 17 descriptors. Better correlations were obtained for k_p than for catalyst activity. Several steric and electronic parameters had significant regression coefficients; thus, Stovneng et al. concluded that catalyst reactivity is a complex function of molecular structure, but they did not report the actual optimized coefficients for the individual QSAR descriptors.

An important descriptor is the steric congestion at the catalytic site due to the presence of the ligands, growing polymer chain, and the counterion. Möhring and Coville reviewed various types of ligand cone angles, solid angles, and other steric descriptors used in a QSAR description.[48] For zirconocenes, ligand cone angles, solid angle, and coordination gap aperture were found to be functionally equivalent, because the catalyst activity decreased linearly with increasing ligand cone angle, increasing solid angle, or decreasing coordination gap aperture.[48,50] Consequently, the monomer accessibility factor γ in eq 20 can also be expanded in terms of the combined ligand solid angle Ω instead of ligand cone angles, where Ω is the solid angle simultaneously subtended by the van der Waals surfaces of all ligands except the growing polymer chain. The monomer accessibility factor γ can be rewritten in terms of solid angle as

$$\gamma = \text{the larger of } (1 - \Omega/(4\pi) - f_\Omega) \text{ or } 0 \qquad (24)$$

where f_Ω is a fitted parameter analogous to the parameter f in eq 21 that accounts for space blocked by the growing polymer chain and partially displaced counterion. Several papers have discussed the merits of ligand cone angles and solid angle as steric descriptors.[48,51] The solid angle offers two potential advantages over ligand cone angles: (a) the solid angle properly accounts for the overlap between the van der Waals surfaces of two or more ligands[52] and (b) the solid angle can be used for bridged ligands where ligand cone angles may not be as useful. A potential disadvantage of solid angle compared to ligand cone angles is that the van der Waals surfaces of the ligands may contain inaccessible crevices which are properly counted as inaccessible space by the ligand cone angles but improperly

(46) (a) Froese, R. D. J.; Musaev, D. G.; Matsubara, T.; Morokuma, K. *J. Am. Chem. Soc.* **1997**, *119*, 7190–7196. (b) Froese, R. D. J.; Musaev, D. G.; Morokuma, K. *Organometallics* **1999**, *18*, 373–379. (c) Vanderlinden, A.; Schaverien, C. J.; Meijboom, N.; Ganter, C.; Orpen, A. G. *J. Am. Chem. Soc.* **1995**, *117*, 3008–3021.

(47) (a) Yao, S.; Shoji, T.; Iwamoto, Y.; Kamei, E. *Comput. Theor. Polym. Sci.* **1999**, *9*, 41–46. (b) Cruz, V. L.; Ramos, J.; Martinez, S.; Munoz-Escalona, A.; Martinez-Salazar, J. *Organometallics* **2005**, *24*, 5095–5102. (c) Cruz, V. L.; Martinez, S.; Martinez-Salazar, J.; Polo-Ceron, D.; Gomez-Ruiz, S.; Fajardo, M.; Prashar, S. *Polymer* **2007**, *48*, 4663–4674. (d) Cruz, V.; Ramos, J.; Munoz-Escalona, A.; Lafuente, P.; Pena, B.; Martinez-Salazar, J. *Polymer* **2004**, *45*, 2061–2072.

(48) Mohring, P. C.; Coville, N. J. *Coord. Chem. Rev.* **2006**, *250*, 18–35.

(49) Stovneng, J. A.; Stokvold, A.; Thorshaug, K.; Rytter, E. In *Metalorganic Catalysts for Synthesis and Polymerization*; Kaminsky, W., Ed.; Springer-Verlag: Berlin, 1999; pp 274−282.

(50) Janiak, C.; Versteeg, U.; Lange, K. C. H.; Weimann, R.; Hahn, E. *J. Organomet. Chem.* **1995**, *501*, 219–234.

(51) (a) Hirota, M.; Sakakibara, K.; Komatsuzaki, T.; Akai, I. *Comput. Chem.* **1991**, *15*, 241–248. (b) White, D.; Taverner, B. C.; Leach, P. G. L.; Coville, N. J. *J. Comput. Chem.* **1993**, *14*, 1042–1049. (c) Tolman, C. A. *Chem. Rev.* **1977**, *77*, 313–348.

(52) Because the van der Waals surfaces of different ligands may overlap, the solid angle subtended by multiple ligands is not necessarily equal to the sum of solid angles subtended by each ligand separately; therefore, the solid angle simultaneously subtended by the multiple ligands should be computed.

counted as accessible space in the solid angle. Since ligand cone angles are easier to compute, they are the preferred steric descriptor if ligand geometry is uncomplicated. Both eqs 21 and 24 contain a steric threshold. Specifically, if

$$(1 - \sin^2(\theta_{Cp'}/4) - \sin^2(\theta_{OAr}/4) - f) < 0 \text{ or } (1 - \Omega/(4\pi) - f_\Omega) < 0 \quad (25)$$

there is not enough room to accommodate the incoming monomer and growing polymer chain, and the predicted polymerization rate drops to 0. For 1-hexene polymerization by Cp′/ArO-ligated Ti catalysts, the steric parameter was $f = 0.187$, which predicts Ti catalysts containing Cp* combined with a ligand sterically larger than OC_6H-2,3,5,6-Ph_4 should not be active for the polymerization of 1-hexene. Janiak et al. reported experimental evidence that qualitatively supports the idea of a steric threshold for zirconocenes, where the activity dropped to slightly above 0 for highly congested catalysts.[48,53]

In summary, ion pair separation energy and steric congestion at the metal center appear to be important descriptors for a wide range of group 4 single-site olefin polymerization catalysts. A structure−activity correlation using DFT-computed ligand cone angles as a measure of steric congestion and E_{IPS} as a measure of ion pair separation difficulty was utilized to explain reactivity changes as a function of metal, ligand, counterion, and solvent for a series of Cp′/ArO-ligated complexes. However, more extensive experimental and theoretical analysis is needed to determine whether the structure−activity correlation of eqs 19 and 20 is applicable to various kinds of group 4 single-site olefin polymerization catalysts in addition to mixed Cp′/ArO complexes.

Acknowledgment. Financial support was provided by the U.S. Department of Energy by Grant No. DE-FG-0203ER15466. The computational resources for the DFT calculations were provided by the National Center for Supercomputing Applications Grant No. MCA04N010 and Information Technology at Purdue (ITaP).

Supporting Information Available: Text, tables, and figures giving experimental details and kinetic analysis and DFT-optimized geometries and energies and CIF files giving X-ray crystal structures for precatalysts **14**, **22**, **24**, and **31**. This material is available free of charge via the Internet at http://pubs.acs.org.

OM8004993

(53) Janiak, C.; Lange, K. C. H.; Versteeg, U.; Lentz, D.; Budzelaar, P. H. M. *Chem. Ber.* **1996**, *129*, 1517–1529.